University of Nevada, Reno

Is evapotranspiration more supplied by summer precipitation or winter precipitation: understanding precipitation sources of terrestrial water use and their variations across wetter and drier years and distinct eco-climatological regions

A thesis submitted in partial fulfillment of the requirements for the degree of

Master of Science in Ecology, Evolution, and Conservation Biology

by

Helen Kesting

Dr. Scott Allen / Thesis Advisor

May, 2023

THE GRADUATE SCHOOL

We recommend that the thesis
prepared under our supervision by

Helen Kesting

entitled

Is evapotranspiration more supplied by summer precipitation or winter precipitation: understanding precipitation sources of terrestrial water use and their variations across wetter and drier years and distinct eco-climatological regions

be accepted in partial fulfillment of the
requirements for the degree of

Master of Science

Scott Allen, Ph.D.
Advisor

Jonathan Greenberg, Ph.D.
Committee Member

Carlos Ramirez-Reyes, Ph.D.
Graduate School Representative

Markus Kemmelmeier, Ph.D., Dean
Graduate School

May, 2023

Abstract 1

The impacts of changing precipitation regimes on the contributions of different seasons' precipitation to evapotranspiration (ET) versus runoff is not well known because empirical insights are scarce. However, such insights are important for improving model predictions of future water-resource availability and ecosystem responses to summer and winter droughts. Here we use using long-term measurements of fluxes and isotope ratios ($\delta^{18}O$) in runoff and precipitation to calculate the partitioning of seasonal precipitation between ET and runoff, using an end-member mixing and splitting framework and focusing on effects of wetter versus drier summers and winters. We hypothesized that drier summers would involve carryover of winter precipitation to mitigate shortages, but related findings were partially indeterminate. However, we did find increases in winter precipitation across a 500-mm range involved the fraction of ET from summer precipitation decreasing from 100% (within error) and the fraction of winter precipitation contributing to ET increasing from 0% (within error) to 21%. Although there were substantial uncertainties in the trends we identified, we expect that the novel approach used here could be a useful framework for understanding the sensitivity of ET partitioning to climatic change, especially where precipitation $\delta^{18}O$ varies substantially between seasons.

Abstract 2

To understand how changing patterns of seasonal precipitation inputs may affect ecosystems and water resources, we need to know how precipitation from different seasons travels through landscapes and contributes to runoff versus evapotranspiration (ET). In this study, we use stable isotope data measured in the National Ecology Observation Network (NEON) aquatic sites to quantify the partitioning of winter and summer precipitation into runoff and ET. Across the 23 watersheds, ranging in size from 1.1 to 47,000 km^2, we found the fraction of summer precipitation routed to ET ranged from 0.13 to 1.00, which coincided with the fraction of ET composed of summer precipitation ranging from 0.04 to 0.76 (readers should note these ranges do not include implausible values generated for 4 sites where the available data were insufficient to constrain uncertainties). To identify factors that influence seasonal precipitation partitioning, a stepwise regression was used with a set of potential predictor variables related to topography, climate, and vegetation. Although many individual variables proved to be significant correlates, 83 % of the variation in the fraction of summer precipitation routed to ET was estimated by a 4-term model using chlorophyll carotenoid index (CCI) variability, mean annual precipitation, and enhanced vegetation indices (EVI) metrics. The fraction of ET sourced from summer precipitation was estimated by the ratio of summer precipitation to annual precipitation and minimum EVI. This is the first cross-site study on seasonal precipitation partitioning, and thus the findings here advance our fundamental understanding of how precipitation is routed to ET versus runoff in differing landscapes.

Acknowledgements

Funding for this study was provided by the Nevada NASA Space Grant Consortium. I would like to thank my advisor, Dr. Scott Allen, for all the time and effort he dedicated to this thesis. I would also like to thank Dr. Jonathan Greenberg and Dr. Carlos Ramirez-Reyes for serving on my committee.

Table of Contents

List of Tables

List of Figures

precipitation was most correlated with minimum EVI (Panel D, R^2=0.61) and the ratio of summer precipitation to annual precipitation (Panel C, R^2=0.52).

Figure 3.3. Observed versus predicted values of the fraction of summer precipitation to ET with observed standard error. Predictions were made using a weighted least squares regression trained on all data except the point being predicted. A 1:1 line is plotted over the range of 0 to 1 to show the bounds of reasonable values for the fraction of summer precipitation to ET.

Figure 3.4. Observed versus predicted values of the fraction of ET from summer precipitation with observed standard error. Predictions were made using a weighted least squares regression trained on all data except the point being predicted. A 1:1 line is plotted over the range of 0 to 1 to show the bounds of reasonable values for the fraction of ET from summer precipitation. The points that fall outside this range appear to have the greatest prediction error, and the negative values are within 2 standard errors of 0.0.

1. Thesis Introduction

Understanding how seasonal inputs of precipitation affect the hydrologic cycle is important for water-resource management and conservation. As seasonal precipitation patterns change with climate change, predicting ecosystem responses will be more feasible if we understand how precipitation from each season is used by vegetation. We can conceptualize a watershed as an open system with inputs of summer and winter precipitation and outputs of runoff and evapotranspiration. By sampling isotope ratios and volumetric fluxes of precipitation and runoff, we can calculate how the two inputs are routed to the two outputs.

End-member mixing is an isotope analysis method used to identify what proportions of a mixture are sourced from two inputs. Building on this method, Kirchner and Allen (2020) developed end-member splitting to identify how two distinct sources are partitioned among a mixture. In this thesis, we utilize these methods to understand how summer and winter precipitation are routed into evapotranspiration (ET), which is the sum of evaporation and plant transpiration (transpiration is typically the much larger term). We call this process precipitation partitioning. This thesis contains two projects: chapter one introduces both projects, chapter two describes the first project which relates to temporal changes in partitioning with interannual variation in seasonal precipitation, chapter three covers the second project which analyzed spatial trends in partitioning relating to climate and vegetation characteristics, and chapter four summarizes both projects.

Chapter two utilizes twenty years of isotope data from the Rietholzbach research catchment in Switzerland to study how partitioning fractions vary based on interannual variations in summer precipitation amount and winter precipitation amount. We use a bootstrapping numerical solution because calculations using annual water-balance closure can be sensitive to uncertainties in the quantification of inputs and outputs. The methods used in this chapter avoid the problematic assumption that precipitation inputs and runoff outputs are confined to a particular water year. This methodology also allows for nonlinear relationships.

Chapter three uses isotope data from 23 National Ecological Observatory Network (NEON) aquatic sites as well as climate and vegetation spatial grid data from a variety of sources. The purpose of this chapter is to gain an initial understanding of potential controls over partitioning fractions. We use stepwise regressions to assess variables relating to precipitation amount and estimates of vegetation vigor calculated from MODIS satellite imagery.

2. Research Chapter 1: Partitioning of seasonal precipitation into runoff and evapotranspiration across wetter and drier years: a case study in the small humid Rietholzbach catchment

2.1. Introduction

The 2018 summer drought in central Europe caused early senescence and mortality in forests, demonstrating forest sensitivity to water deficits in the often-humid regions of central Europe (Schuldt et al., 2020; Arend et al., 2021). Summer droughts are expected to be more frequent across Europe and North America with climate change (Lotsch et al., 2005). Although vegetation, especially long-lived trees, can avoid drought by senescing early or taking up stored subsurface waters from previous seasons, predicting the effects of hydroclimatic variability on vegetation and evapotranspiration (ET) fluxes requires better understanding the fates of seasonal precipitation across years with wetter-or-drier summers and wetter-or-drier winters. Stable isotopes of oxygen and hydrogen in water are ideal tracers to address seasonal precipitation partitioning and these isotope ratios are among the numerous metrics characterized for routinely collected water samples. Here, we use $\delta^{18}O$ which is calculated from the ratio of heavier oxygen-18 to lighter oxygen-16 relative to a global standard isotope ratio. While $\delta^{18}O$ from xylem water or tissue has been used to determine the relative use of summer versus winter precipitation by individual plants (Martin et al., 2018; Berkelhammer et al., 2020; Goldsmith et al., 2022; Ehleringer et al., 1991), end-member splitting can be

used to directly examine fate of precipitation at watershed scales (Kirchner and Allen, 2020).

End-member splitting addresses the question, “how much of input sources X and Y are in an output mixture”, unlike the question addressed by end-member mixing, “what is the proportion of inputs X and Y in the output mixture”. This method has been used in several previous studies to address the splitting of winter versus summer precipitation, rain versus snow, or precipitation generating high versus low flows into runoff and ET components of the water budget (Allen et al., 2019; Sprenger et al., 2022a; Sprenger et al., 2022b). Kirchner and Allen (2020) found that summer precipitation (April-November) dominated ET at the Hubbard Brook Experimental Forest in New Hampshire. In snow-dominated mountainous watersheds of the western US, Sprenger et al. (2022a) found that the fraction of snow routed to ET varied among years from 100% to less than 20%, and the fraction of ET from snow did not vary systematically with snowfall amounts. Alternatively, in a Mediterranean watershed, summer precipitation or low-runoff-generating precipitation more efficiently contributed to ET than winter or high-runoff-generating precipitation, respectively (Sprenger et al., 2022b). A related but less-quantitative method has shown that summer and winter precipitation were approximately equally represented in streamflow in 12 watersheds throughout Switzerland, suggesting that neither season’s precipitation was consistently over- or under-represented in ET (Allen et al., 2019).

The objective of this study is to determine seasonal precipitation contributions to ET and their sensitivity to changes in precipitation inputs. We use long-term hydrologic records and isotope data collected at the Rietholzbach catchment in Switzerland. We hypothesized that 1) ET is primarily composed of summer precipitation because ET mostly occurs in summer, 2) the fraction of ET sourced from summer precipitation decreases in drier summers, 3) the contributions of winter precipitation to ET increase in drier summers to compensate for summer precipitation shortages. If the use of winter precipitation fully compensates for summer precipitation shortages, inter-seasonal precipitation carryover would represent a mechanism of ecosystem resistance to summer drought in this climate where annual ET likely very rarely exceeds annual precipitation. In pursuing these hypotheses, we also tested how amounts of winter precipitation, independent of variations in summer precipitation amount, affect seasonal precipitation partitioning.

2.2. Methods

Section 2.2.1 defines end-member mixing and splitting methods and equations. In sections 2.2.2 and 2.2.3, we'll briefly summarize the Rietholzbach catchment landscape and climate, then we'll describe the dataset. In section 2.2.4, we'll explain how we managed data gaps and how we calculated values used in end-member splitting. Section 2.2.5 describes the statistical methods used to analyze end-member splitting results.

2.2.1. End-Member Mixing and Splitting

The end-member splitting method introduced by Kirchner and Allen (2020) goes beyond end-member mixing (which addresses the relative fraction of each end-member in a mixture) by also making use of mass-flux data to address how each end-member is partitioned among its different fates. In the case of this study, the two input end-members are summer and winter precipitation (P_S and P_W) with mean $\delta^{18}O$ ratios $\bar{\delta}_{P_S}$ and $\bar{\delta}_{P_W}$ and the measured mixture is either annual runoff (Q) with mean $\delta^{18}O$ defined by $\bar{\delta}_Q$ or seasonal runoff (Q_S and Q_W) with mean $\delta^{18}O$ defined by $\bar{\delta}_{Q_S}$ and $\bar{\delta}_{Q_W}$. We can use end-member mixing and splitting equations to calculate the fraction of seasonal runoff sourced from summer precipitation (eq. 2.1) and the fraction of summer precipitation routed to seasonal runoff (eq. 2.2).

$$f_{\mathrm{Qs}\leftarrow\mathrm{Ps}} = \frac{\bar{\delta}_{Q_S} - \bar{\delta}_{P_W}}{\bar{\delta}_{P_S} - \bar{\delta}_{P_W}} \qquad f_{\mathrm{Qw}\leftarrow\mathrm{Ps}} = \frac{\bar{\delta}_{Q_W} - \bar{\delta}_{P_W}}{\bar{\delta}_{P_S} - \bar{\delta}_{P_W}} \tag{2.1}$$

$$\eta_{\mathrm{Ps}\rightarrow\mathrm{Qs}} = \frac{\mathrm{Qs}}{\mathrm{Ps}} \frac{\bar{\delta}_{Q_S} - \bar{\delta}_{P_W}}{\bar{\delta}_{P_S} - \bar{\delta}_{P_W}} \qquad \eta_{\mathrm{Ps}\rightarrow\mathrm{Qw}} = \frac{\mathrm{Qw}}{\mathrm{Ps}} \frac{\bar{\delta}_{Q_W} - \bar{\delta}_{P_W}}{\bar{\delta}_{P_S} - \bar{\delta}_{P_W}} \tag{2.2}$$

To calculate the partitioning of seasonal precipitation into evapotranspiration (ET) and runoff, we use annual runoff as the measured mixture. By solving for the fraction of each seasons' precipitation that contributes to runoff ($\eta P_S \rightarrow Q$ or $\eta P_W \rightarrow Q$), we can also solve for the fractions of each season's precipitation missing from runoff, which we assume to represent ET at long time scales (assuming steady-state storage volumes and isotope ratios and no inter-basin subsurface flows). By this logic, we

calculate both the mixing solution, the fraction of ET from summer precipitation ($fET \leftarrow P_S$):

$$f_{ET \leftarrow P_S} = \frac{P_S - Q \; fQ \leftarrow P_S}{ET} = \frac{P_S - Q \frac{\bar{\delta}_Q - \bar{\delta}_{P_W}}{\bar{\delta}_{P_S} - \bar{\delta}_{P_W}}}{P_S + P_W - Q} \quad (2.3)$$

as well as the splitting solution, the fraction of summer precipitation to ET ($\eta P_S \rightarrow ET$):

$$\eta_{P_S \rightarrow ET} = \frac{ET}{P_S} \; fET \leftarrow P_S = 1 - \eta_{P_S \rightarrow Q} = 1 - \frac{Q}{P_S} \; fQ \leftarrow P_S = 1 - \frac{Q}{P_S} \frac{\bar{\delta}_Q - \bar{\delta}_{P_S}}{\bar{\delta}_{P_S} - \bar{\delta}_{P_S}} \quad (2.4)$$

The amount of summer precipitation routed to ET is calculated by multiplying $\eta P_S \rightarrow ET$ by the amount of summer precipitation. Standard errors of partitioning fractions were calculated using gaussian error propagation (see Kirchner and Allen, 2020, and the associated supplemental file).

2.2.2. Site and Dataset Description

Rietholzbach is a small research watershed in northeastern Switzerland (47.38°N, 8.99°E) with an area of 3.31 km^2. The elevation ranges from 682 to 950 m a.s.l. with a mean of 795 m a.s.l. The watershed is mostly covered in pastureland (71.9 %) with small patches of forest (25.6 %) and minimal non-vegetated area (Seneviratne et al., 2012).

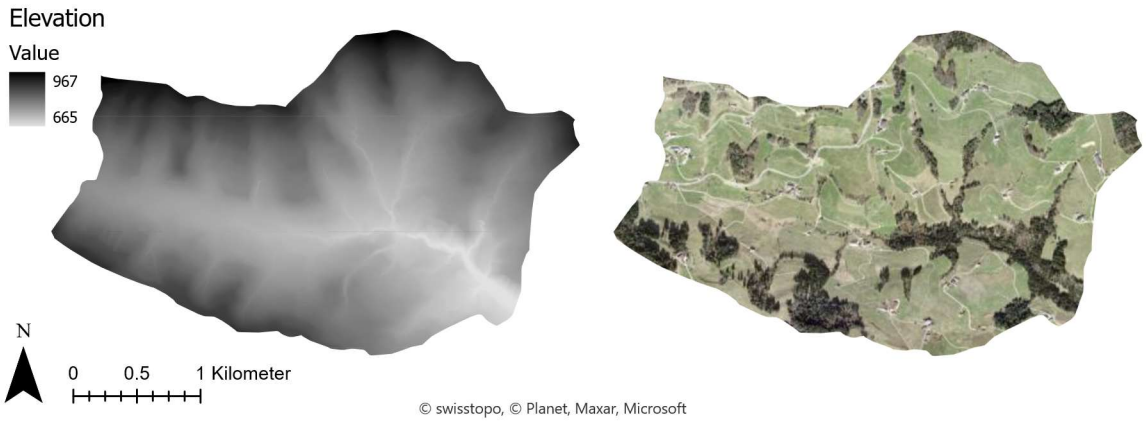

Figure 2.1. Two maps of the Rietholzbach watershed showing elevation from the Swiss Federal Office of Topography and satellite imagery from Planet, Maxar, and Microsoft.

This study analyzes data collected from three control volumes defined by three runoff isotope datasets: a) a lower gauge at the watershed outlet measures runoff over the entire 3.3-km^2 watershed (All RHB), b) a higher-elevation gauge defines a 1.6-km^2 sub-watershed with a mean elevation of 818 m a.s.l. (Upper RHB), and c) a weighing lysimeter at 755 m a.s.l. measures mass and seepage from a grass-covered cylinder of soil with a 3.14-m^2 area and a 2.5-m depth. The weighing lysimeter is located near the upper gauge, and it is collocated with an eddy-covariance tower and precipitation gauge. Albeit unimportant for the isotope time series, evidence suggested that runoff at the Upper RHB gauge was under-estimated when compared to the All RHB data; area-adjusted runoff from the lower gauge was used to analyze both isotope datasets.

The mean monthly air temperature ranges from -0.5°C in January to 16.5°C in July (1994-2014). Across the study years, long-term mean annual precipitation was 1453 mm y^{-1} for All RHB (1994-2009) and 1465 mm y^{-1} for Upper RHB and the lysimeter (1994-2014), with a long-term mean of 50 – 52 % falling in summer (May to September) and 48

– 50 % falling in winter (October to April); readers should note that summer is here defined as a 5-month season and winter as a 7-month season, thus monthly precipitation rates are higher in summer. The same precipitation gauge was used as an estimate of precipitation in all three study units. Over those same respective years (1994-2009 for All RHB and 1994-2014 for Upper RHB and the lysimeter), long-term mean runoff was measured as 990 mm y^{-1} for All RHB, estimated as 993 mm y^{-1} for Upper RHB (using lower-gauge data), and measured as 1047 mm y^{-1} for the lysimeter. By mass-balance closure, long-term mean ET was 463 mm y^{-1} for All RHB, 472 mm y^{-1} for Upper RHB, and 418 mm y^{-1} for the lysimeter.

The Rietholzbach streamflow records, stream and groundwater chemistry records, lysimeter measurements, and meteorological data have informed numerous studies to address questions about controls over streamflow generation (Vitvar and Balderer, 1997; von Freyberg et al., 2015), flow through porous media (Beven and Germann, 1982), and ET (Michel and Seneviratne, 2022; Seneviratne et al., 2012; Teuling et al., 2010; Hirschi et al., 2017).

2.2.3. Data Sources and Preprocessing

The primary data used in this study comprise measurements of flux amounts and isotopic compositions for precipitation inputs and runoff outputs, for All RHB, Upper RHB, and the lysimeter. We also used lysimeter evapotranspiration data reported by Hirschi et al. (2017).

Oxygen isotope ratios ($\delta^{18}O$) of water were available from November 1993 to February 2010 for All RHB, and from November 1993 to January 2015 for the precipitation gauge, the lysimeter seepage, and Upper RHB streamflow. Precipitation $\delta^{18}O$ measurements included all precipitation that fell during the study period, whereas streamflow $\delta^{18}O$ measurements were from grab samples. All samples were collected at two-to-four-week intervals, and volumetric fluxes of precipitation, runoff, and lysimeter seepage were reported at daily resolution. Long-term ET was calculated at annual resolution through water-balance closure using precipitation and runoff by assuming that storage is in steady state (All RHB and Upper RHB) or at monthly resolution for the lysimeter by using daily changes in lysimeter mass balance (Figure S1). Further site characteristics and measurement systems are reported in Seneviratne et al. (2012).

Initial pre-processing and quality control measures were conducted because the isotope data were collected over decades and were analyzed using different instrumentation. Most of the $\delta^{18}O$ values were analyzed by isotope ratio mass spectrometry using the CO_2 equilibration method (Vitvar and Balderer, 1997; Oertel, 2016; Lehner et al., 2009), but four years of samples (2002-2003, 2013-2014) were analyzed using a laser spectroscopy system (Picarro L2130-i, California, USA). All isotope data are expressed in per mil (‰) notation relative to V-SMOW. Although no $\delta^{2}H$ data were used in our study, the data segments analyzed using the Picarro analyzer (which also yields $\delta^{2}H$ data) have been previously reported (Oertel, 2016); Oertel used those

data as evidence that there was no substantial evaporative fractionation in watershed-runoff or lysimeter-seepage data.

2.2.4. Data Processing

To conduct end-member splitting, the end-members were defined by two seasons: winter (October to April) and summer (May to September). This was done for the dataset as a whole and for each hydrologic year starting in October. The lysimeter flux record was missing 12 days out of 7,305 total (Figure S2). The gaps were filled using bi-weekly averages which were recorded with each isotope measurement.

To calculate weighted mean isotope values, each measurement was assigned a weight according to the flux size (cumulative precipitation amount or daily runoff rate). When a precipitation sampling interval spanned two seasons, the isotope value for that interval contributed to the means for both seasons, with its weight respective to the sum of daily precipitation amounts for the days in each season. Runoff and precipitation sampling intervals with missing isotope values were ignored (8.6 % of precipitation records, 3.0% of All RHB runoff records, 1.9% of Upper RHB runoff records, and 1.1% of lysimeter seepage records; Figure S2).

Weighted mean isotope values (Figure S3) used in long-term endmember splitting (Figure 2.1) were calculated using data from October 1994 through September 2009 for All RHB and October 1994 through September 2014 for precipitation, Upper RHB, and the lysimeter. Weighted mean isotope values used in annual end-member

splitting (Figures 2.3-2.5) were calculated using data from October through September of each year, for the years stated above.

2.2.5. Statistical Analysis

The following analyses were conducted using Python 3.9 (van Rossum and Drake, 2009) in PyCharm2021.2.1. Data processing of each dataset (All RHB, Upper RHB, and Lysimeter) resulted in long-term (Figure 2.2) and annual (Figures 2.3-2.5) values for the variables in equations 1 through 4. We also categorized the annual data into water years with greater than versus less than the median summer or winter precipitation amount. End-member splitting analysis was then conducted using the sum of fluxes and the weighted average of isotope values from each category (Figure 2.3).

To quantify partitioning across the range of observed seasonal precipitation amounts (Figures 2.4-2.5), we modeled runoff sources (mixing analyses) and precipitation partitioning (splitting analysis) by substituting each term of equations 2.1 through 2.4 with fitted linear regressions of each term as a function of summer or winter precipitation. Scatterplots of those data are shown in Figures S7-S12, with those data randomly resampled in a bootstrapping routine to propagate linear regression errors through to the splitting and mixing results; the bootstrapping involved 3000 iterations of sampling 20 points (or 15 for All RHB) with replacement. While not all terms showed a statistically significant relationship with summer or winter precipitation amount, we remind readers that using fitted regressions is more accurate than using mean values.

Annual ET calculated by water balance was less consistent than ET calculated from lysimeter mass variations (Figure S1). For ET partitioning solutions (eq. 2.3 and 2.4, Figure 2.5), we refined our calculations of annual ET and runoff. Instead of closing the water budget annually, we estimated net percolation because the partitioning examined here occurs in the terrestrial critical zone, rather than in deep groundwaters that largely supply runoff. This was done by rescaling the inferred watershed-scale ET to match interannual variations in ET as calculated from lysimeter mass variations, but still closing the water balance across the full study duration (and thereby not violating mass conversion laws). This method dampened interannual variations in ET such that they better match the direct measurements quantified from lysimeter mass variations in which storage changes can be accounted for (Figure S1). To ensure water-balance closure for each year, we also subtracted annual precipitation by lysimeter-scaled annual ET to recalculate annual runoff.

2.3. Results and Discussion

2.3.1. Long-Term Average Precipitation Partitioning

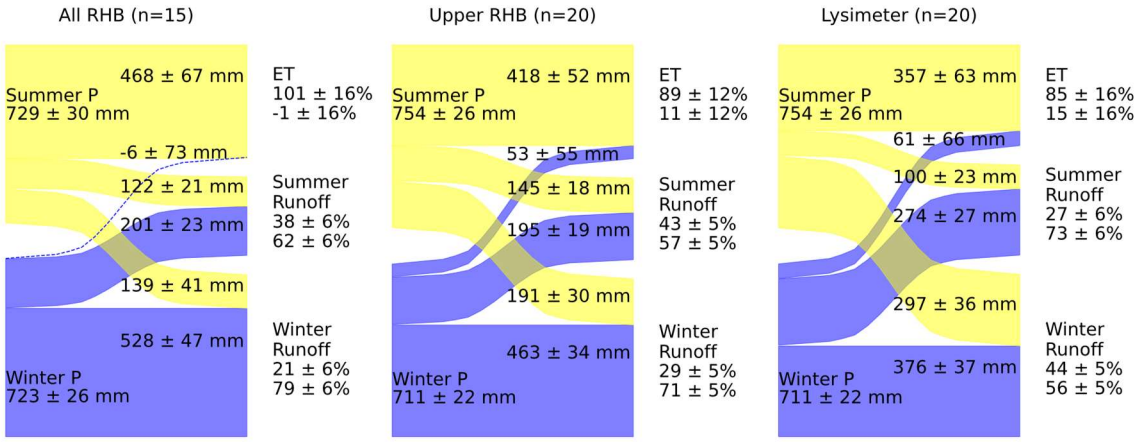

Figure 2.2. Summer and winter precipitation split into evapotranspiration, summer runoff, and winter runoff for the entire watershed (All RHB), the upper sub-watershed (Upper RHB), and the lysimeter. Partitioning was calculated over the entire study period using measured flux amounts. Values are shown as annual averages with standard error. Yellow represents fluxes from summer precipitation and blue represents fluxes from winter precipitation. The thickness of each line corresponds to the flux amount. Dashed lines represent negative averages. For each output end-member, the percentage sourced from summer versus winter precipitation is shown on the right. Evapotranspiration was predominantly composed of summer precipitation. Both summer and winter runoff were composed of mostly winter precipitation.

Across the entire records, among all three datasets (Figure 2.2), a substantial fraction of summer precipitation becomes ET (64 ± 9 % for All RHB, 55 ± 7 % for Upper RHB, 47 ± 8 % for Lysimeter (values are reported as mean ± 1SE, here and throughout Section 2.3). Much less summer precipitation becomes summer runoff (17 ± 3 % for All RHB, 19 ± 2 % for Upper RHB, 13 ± 3 % for Lysimeter) or winter runoff (19 ± 6 % for All RHB, 25 ± 4 % for Upper RHB, 39 ± 5 % for Lysimeter). In contrast, a negligible fraction of winter precipitation became ET (-1 ± 10 % for All RHB, 8 ± 8 % for Upper RHB, 9 ± 9 % for Lysimeter). Larger fractions of winter precipitation became summer runoff (28 ± 3 % for

All RHB, 27 ± 3 % for Upper RHB, 38 ± 4 % for Lysimeter) and the majority became winter runoff (73 ± 6 % for All RHB, 65 ± 5 % for Upper RHB, 53 ± 5 % for Lysimeter). Accordingly, annual ET was inferred to be predominantly composed of summer precipitation, showing mixing fractions within 1 SE of 100%: 101 ± 16 % for All RHB, 89 ± 12 % for Upper RHB, and 85 ± 16 % for Lysimeter. Winter precipitation was the majority source for both winter runoff (79 ± 6 %, 71 ± 5 %, and 56 ± 5 %) and summer runoff (62 ± 6 %, 57 ± 5 %, and 73 ± 6 %), for All RHB, Upper RHB, and Lysimeter, respectively).

These long-term results imply that ET and thus also transpiration is minimally supplied by winter precipitation, on average. However, even with the average percentages of ET from summer precipitation all being indistinguishable from 100%, it is possible that winter precipitation contributed more to ET in some years. Although the partitioning diagrams for All RHB, Upper RHB, and Lysimeter may appear visually similar (Figure 2.2), the relative partitioning of seasonal precipitation to seasonal runoff differed. Lysimeter summer runoff contained the highest percent of winter precipitation of the three datasets, whereas lysimeter winter runoff contained the lowest. This reflects the approximately 6-month phase shift between lysimeter seepage isotopes and precipitation isotopes visible in Figure S3 (and previously described by Vitvar and Balderer, 1997), and it highlights the challenge in using a lysimeter to examine catchment-scale soil-water transport conditions. Given the similarity between the two watersheds and the longer record for Upper RHB, the rest of Sections 2.3 and 2.4 focus

on Upper RHB unless otherwise specified. Results for All RHB and the lysimeter are reported in Appendix 1.

The biases of ET toward using summer precipitation and of runoff toward using winter precipitation are not entirely unexpected. ET was found to be mostly composed of summer precipitation at Hubbard Brook Experimental Forest (Kirchner and Allen, 2020) using data collected by Campbell and Green (2019). Jasecko et al. (2014) showed that groundwater recharge is biased toward winter precipitation in temperate forests which supports our findings that runoff is primarily composed of winter precipitation (66 %). The bias of runoff toward using winter precipitation has been argued for in previous studies at Rietholzbach (Vitvar and Balderer, 1997).

2.3.2. Precipitation Partitioning in Water Years with Drier Versus Wetter Summers and in Water Years with Drier Versus Wetter Winters

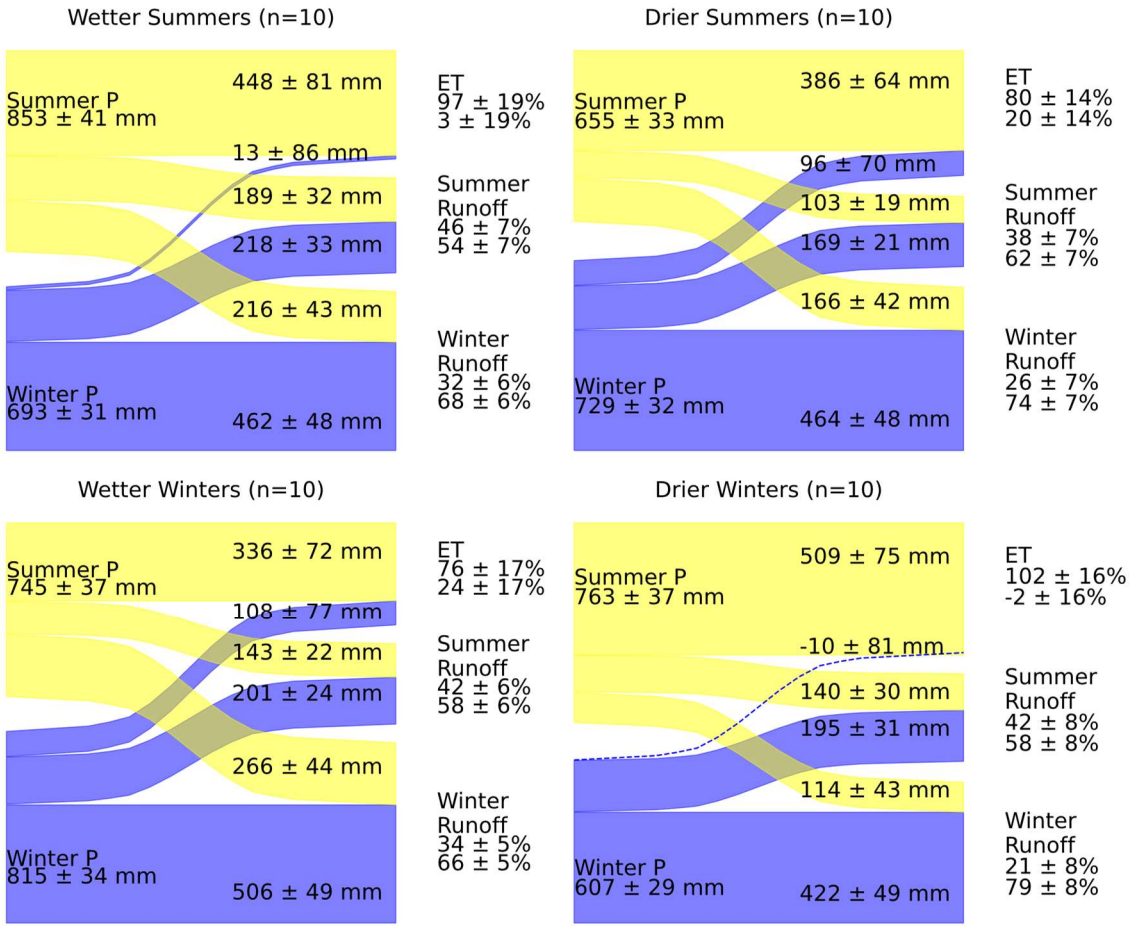

Figure 2.3. Summer and winter precipitation split into evapotranspiration, summer runoff, and winter runoff for the years in which summer precipitation was greater than versus less than the median summer precipitation amount and for years in which winter precipitation was greater than versus less than the median winter precipitation amount using the upper sub-watershed (Upper RHB) dataset. Values are shown as annual averages with standard error. Yellow represents fluxes from summer precipitation and blue represents fluxes from winter precipitation. The thickness of each line corresponds to the flux amount. Dashed lines represent negative averages. For each output end-member, the percentage sourced from summer versus winter precipitation is shown on the right. When comparing wet-summer years to dry-summer years or wet-winter years to dry-winter years, the only significantly different partitioning fraction was the decrease in the fraction of summer precipitation to winter runoff in dry-winter years ($p = 0.02$).

In wet-summer years (i.e., water years exceeding the median summer precipitation amount), ET amount averaged 461 ± 58 mm with 97 ± 19 % from summer

precipitation which was not significantly different from dry-summer years in which ET averaged 482 ± 51 mm with 80 ± 14 % from summer precipitation ($p > .05$, Figure 2.3). All p-values reported in section 2.3.2 are from two-sided t-tests with 18 degrees of freedom. While the mixing and splitting fractions were similar between wet-summer and dry-summer years, some of the flux amounts differed. In wet-summer years, the average summer runoff amount was 406 ± 18 mm, whereas in dry-summer years the summer runoff amount decreased to 272 ± 12 mm ($p < .001$) and the amount of summer precipitation to summer runoff also decreased ($p = .03$). Fluxes to winter runoff were similar among wet-summer and dry-summer years ($p > .05$).

In wet-winter years (i.e., water years exceeding the median winter precipitation amount), ET amount averaged 444 ± 57 mm with 76 ± 17 % sourced from summer precipitation which was not significantly different from dry-winter years in which ET averaged 500 ± 51 mm with 102 ± 16 % sourced from summer precipitation ($p > .05$, Figure 2.3). We were unable to reject the null hypothesis ($p = .11$) regarding whether less summer precipitation supplies ET in wet-winter years (336 ± 72 mm) than in dry-winter years (509 ± 75 mm). In wet-winter years winter runoff averaged 772 ± 22 mm whereas in dry-winter years winter runoff decreased to 536 ± 15 mm ($p < .001$) and the fraction of summer precipitation to winter runoff also decreased ($p = .02$). Fluxes to summer runoff were similar among wet-winter and dry-winter years ($p > .05$).

2.3.3. The Dependence of Precipitation Partitioning on Summer and Winter Precipitation Amounts

The non-linear function that results from substituting linear functions of summer precipitation or winter precipitation into equations 2.1 through 2.4 precludes significance tests on the fitted function's coefficients as would typically be done to evaluate the significance of linear functions; however, statistical differences can be compared at specific places along the curves in Figures 2.4 and 2.5. P-values in section 2.3.3 represent the percent of bootstrapping iterations in which there was a consistent increasing or decreasing trend. For example, in 2887 of the 3000 bootstrapping iterations ($p = .04$), the fraction of summer precipitation that becomes summer runoff increased when comparing 500 mm of summer precipitation to 1000 mm of summer precipitation (Figure 2.4E). The amount of summer precipitation to summer runoff also increases over the same range of summer precipitation values ($p = .01$, Figure 2.4K). While these results are supported by the increase in summer runoff amount (Figure S7E), they should be interpreted with caution since the decrease in $\delta^{18}O$ of summer precipitation with wetter summers (Figure S7A) could be exaggerating this trend. This is the only flux that showed a significant trend with summer precipitation amount (Figures 2.4 and 2.5).

When comparing 500 mm of winter precipitation to 1000 mm of winter precipitation, the fraction of summer runoff sourced from summer precipitation increased ($p = .03$, Figure 2.4C) as did the fraction of summer precipitation routed to

summer runoff ($p = .03$, Figure 2.4F). This could represent “flushing” of the previous summer’s precipitation via piston-flow dynamics or preferential flow of recent summer precipitation after wet winters. Over the same range, the fraction and amount of summer precipitation that becomes winter runoff also increased ($p = .01$ and $p = .02$, respectively, Figures 2.4D and 2.4J). Surprisingly, the fraction and amount of winter precipitation that becomes summer runoff decreased over the same range ($p = .002$ and $p = .047$, Figures 2.4I and 2.4O). Since winter precipitation amount is not correlated with the fraction of precipitation falling as snow (Figure S4B) or February through April mean temperature (Figure S4D), this is not likely due to dry winters potentially having more seasonal carryover of winter precipitation as snowpack.

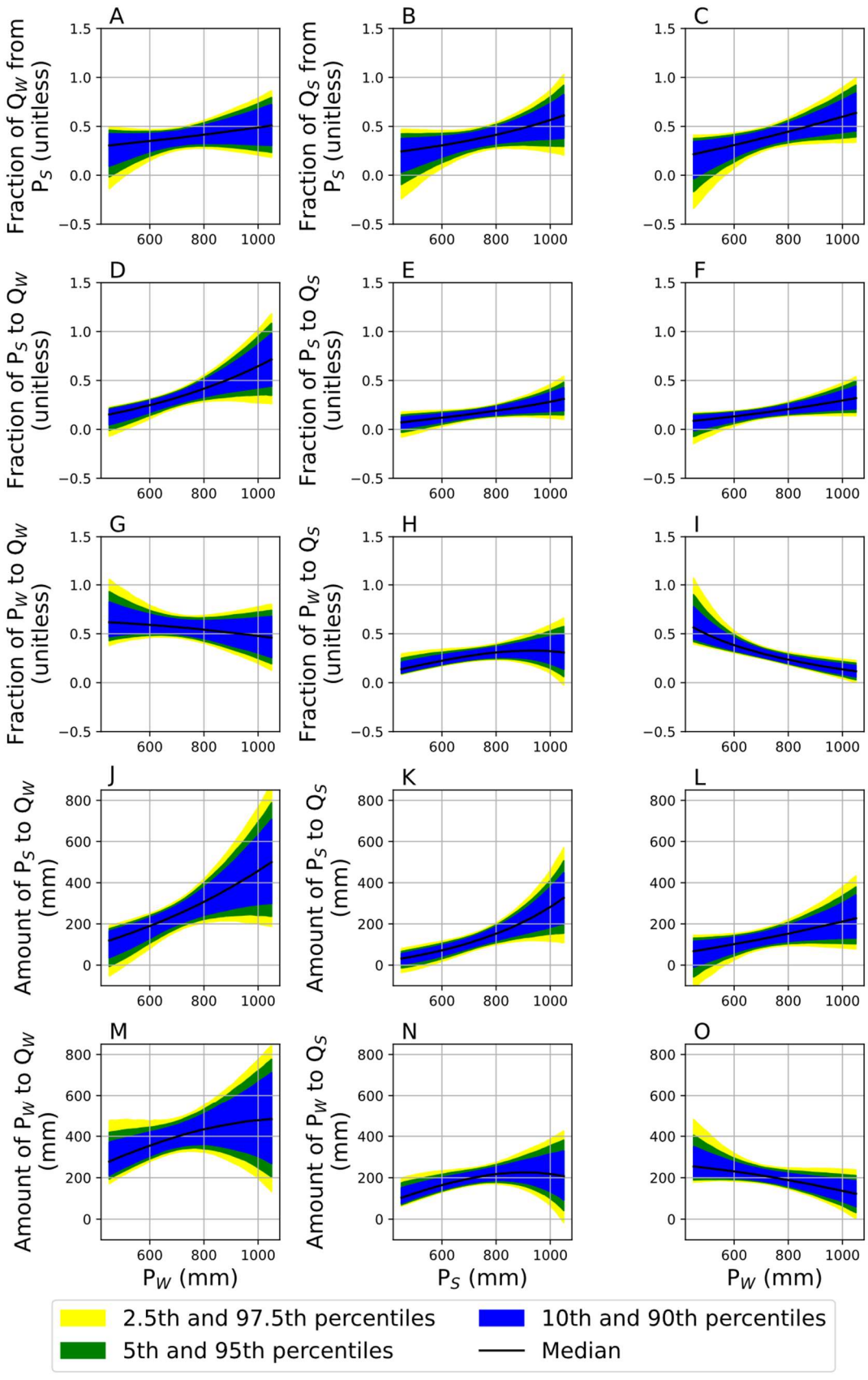
A
B
C
D
E
F
G
H
I
J
K
L
M
N
O
Fraction of Q_W from P_S (unitless)
Fraction of Q_S from P_S (unitless)
Fraction of P_S to Q_W (unitless)
Fraction of P_S to Q_S (unitless)
Fraction of P_W to Q_W (unitless)
Fraction of P_W to Q_S (unitless)
Amount of P_S to Q_W (mm)
Amount of P_S to Q_S (mm)
Amount of P_W to Q_W (mm)
Amount of P_W to Q_S (mm)
P_W (mm)
P_S (mm)
P_W (mm)
2.5th and 97.5th percentiles
10th and 90th percentiles
5th and 95th percentiles
Median

Figure 2.4. Fractions and amounts of precipitation partitioning into summer and winter runoff with summer precipitation (P_S) in mm and winter precipitation (P_W) in mm on the x-axis. These plots only show data from Upper RHB. Because of the definition of water years as October to September, this figure excludes winter runoff generation as a function of summer precipitation. Such data introduce potential misinterpretations as the summer precipitation should not be interpreted as a control over the winter runoff that precedes it. However, this does not invalidate the interpretations of the amounts and fractions of summer precipitation in winter runoff because the mean absolute deviation of summer precipitation isotope values (0.86 ‰) is substantially smaller than the average inter-seasonal range of 3.42 ‰ (Figure S3) and, moreover, those variations are not detectably related to winter precipitation amounts (Figure S8A). The relationships that are hard to justify in Figure S7 (S7B, S7D, S7F, S7I) are non-significant and thus there is no implied dependence of winter precipitation and runoff on summer precipitation that has not yet occurred. Therefore, using and propagating those relationships is simply appropriately introducing and tracking uncertainties.

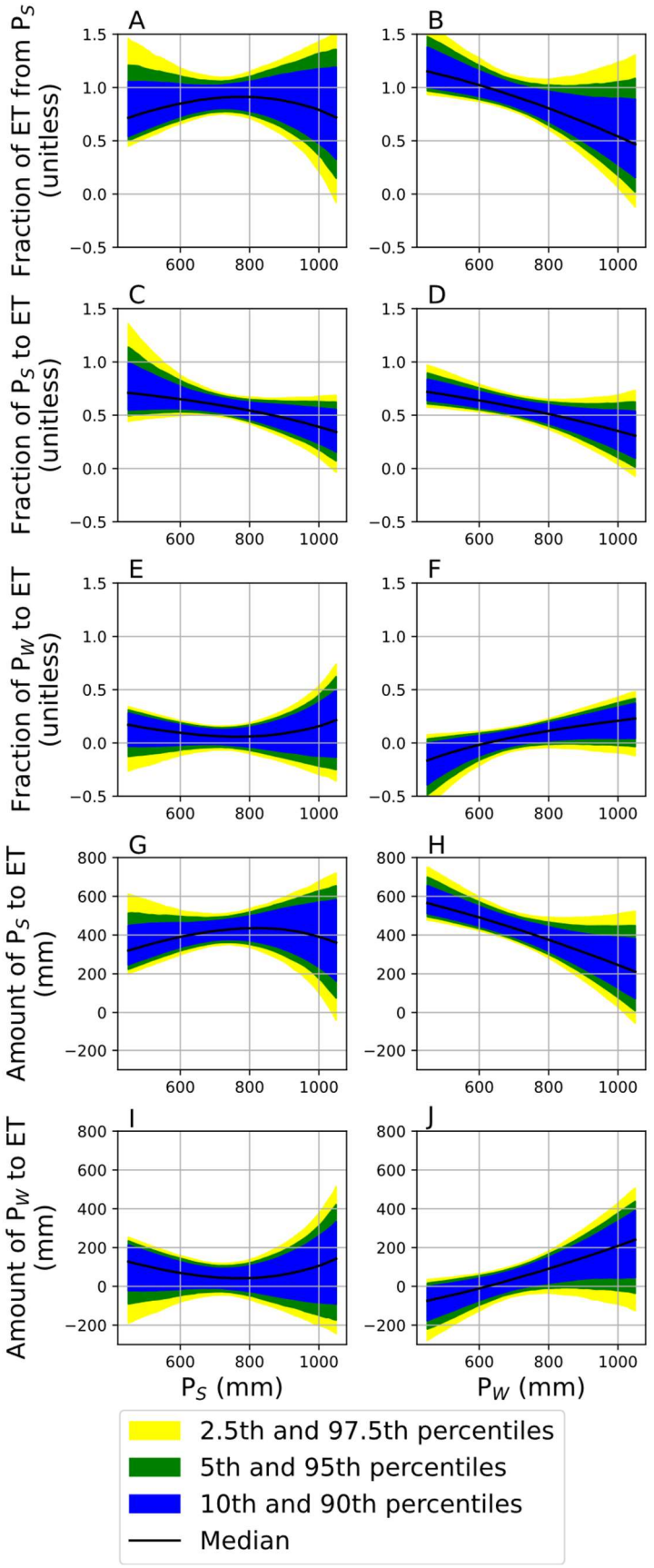
A
B
C
D
E
F
G
H
I
J
Fraction of ET from P_S (unitless)
Fraction of P_S to ET (unitless)
Fraction of P_W to ET (unitless)
Amount of P_S to ET (mm)
Amount of P_W to ET (mm)
P_S (mm)
P_W (mm)
2.5th and 97.5th percentiles
5th and 95th percentiles
10th and 90th percentiles
Median

Figure 2.5. Fractions and amounts of precipitation partitioning into evapotranspiration (ET) with summer precipitation (P_S) in mm and winter precipitation (P_W) in mm on the x-axis. These plots only show data from Upper RHB.

None of the ET partitioning fractions were significantly correlated with summer precipitation amount ($p > .05$, Figure 2.5). The fraction and the amount of summer precipitation to ET decreased with an increase in winter precipitation from 500 mm to 1000 mm ($p = .04$ and $p = .03$, respectively, Figures 2.5D and 2.5H). Since uncertainty increases at high precipitation values, a greater number of relationships were significant over the winter precipitation range of 500 mm to 800 mm. Over this range, the fraction and amount of winter precipitation to ET increased ($p = .04$ for both Figures 2.5F and 2.5J) and the fraction of ET from summer precipitation decreased ($p = .04$, Figure 2.5B). Since ET amount was not correlated with summer or winter precipitation amount (Figures S7J and S8J), tradeoffs in the use of different sources appear to represent a mechanism by which ET demand is still satisfied (at least, at this site over the range of conditions observed). Readers may note that most of the iterated values shown by the confidence intervals sit outside of the range of possible fractions (i.e., 0-to-1) for some sections of the domain, but they are never significantly outside of the range ($p > .05$).

The data suggest that winter precipitation controls the source partitioning of ET with wetter winters increasing the fraction and amount of winter precipitation to ET, decreasing the fraction and amount of summer precipitation to ET, and decreasing the fraction of ET from summer precipitation. Since the fraction of winter precipitation to winter runoff does not vary significantly with winter precipitation ($p > .05$, Figure 2.4G), the increase in the fraction of winter precipitation to ET with wetter winters is balanced

by a decrease in the fraction of winter precipitation to summer runoff. Though the mechanism underlying this trend is unclear, the partitioning calculations are likely driven by the increase in $\delta^{18}O$ of summer runoff in water years with wetter winters (Figure S8C).

2.3.4. Further Discussion of Uncertainties and Technical Considerations

Calculations using annual water-balance closure can be sensitive to uncertainties in the quantifications of inputs or outputs. Because the method's assumptions are imperfect, there is substantial noise in the trends of partitioning fractions across individual years. Using the dampening and phase shift of precipitation isotope signals in runoff, von Freyberg et al. (2018) estimated the flow-weighted young water fraction (the proportion of runoff younger than approximately 2–3 months) as 0.2 for All RHB and 0.13 for Upper RHB. This suggests that there is substantial inter-annual carryover of water in subsurface storage. The methods used in this paper avoid the problematic assumption that precipitation inputs and runoff outputs are confined to a particular water year. Furthermore, this method allows for nonlinear relationships which are suggested by the correlations between variables in eq. 2.1–2.4 (Figures S7 and S8).

For the results reported above, $\delta^{18}O$ values were not corrected for the precipitation gauge being located at a lower elevation than the watersheds' mean elevations, introducing a potential bias in $\delta^{18}O$ values. Assuming the global average isotopic lapse rate of ~0.28‰ $\delta^{18}O$/ 100 m (Poage and Chamberlain, 2001), we decreased all precipitation $\delta^{18}O$ values by 0.12‰ for All RHB and by 0.18‰ for Upper

RHB, then repeated the calculations shown in Figure 2.2. The fraction of ET from summer precipitation decreased by 8% for All RHB and 11% for Upper RHB. We did not apply this method to the lysimeter dataset because the lysimeter is at the same elevation as the precipitation gauge. Elevation effects should not affect trends with seasonal precipitation amounts because all precipitation isotope values are adjusted by the same amount.

Seneviratne et al. (2012) estimates up to 15% undercatch of rain and up to 50% undercatch of snow. Using these maximum estimates, we increased each precipitation measurement by 15% if the temperature was above 2°C and by 50% if the temperature was at or below 2°C (9.6% of annual precipitation, 1994-2014). We tested the potential impact of undercatch by repeating the calculations shown in Figure 2.2 with adjusted precipitation data. The fraction of ET from summer precipitation decreased by 23%, 18%, and 18% for All RHB, Upper RHB, and the lysimeter, respectively, and the fraction of summer precipitation routed to ET increased by 4%, 5%, and 6%. Precipitation undercatch should not affect the partitioning trends observed because summer and winter precipitation amounts are not significantly related to the fraction of precipitation falling as snow (Figures S4A and S4B).

2.4. Synthesis and Conclusions

We found greater fractions of winter precipitation (92%, Upper RHB long-term mean) than summer precipitation (45%) became streamflow at Rietholzbach, contrasting with the Allen et al. (2019) finding that approximately equal fractions of

both summer and winter precipitation are represented in ET in 12 watersheds throughout Switzerland; however, Rietholzbach has a relatively high precipitation input among location locations that are not snow-dominated or montane. Snow dominated regions seem to show more precipitation routed to ET in high-elevation regions, as demonstrated by Sprenger et al. (2022a) who used isotopes to study the partitioning of snow and rain in 9 catchments in the Upper Colorado River Basin; across catchments, they found that 33% of snow was routed to ET, with the rest coming from rain. That same study also found that variation among catchments was affected by vegetation, and the fraction of ET from snow increased with tree density. Rietholzbach is a mostly grass-dominated site, perhaps explaining why the watershed's findings are not consistent with those of Allen et al. (2019). That said, in drier climates with sparse trees, such as in the Spanish Pyrenees, ET has been shown to be composed of 45±5% winter (October-April) precipitation and 55±5% summer (May-September) precipitation (Sprenger et al. (2022b). Insufficient analyses of these types exist to yet support comparative insights, however (but see Section 3 of this thesis).

Others have used stable isotopes to address similar questions but using different approaches. For example, Kleine et al. (2021) used a tracer-aided ecohydrological model to find that winter precipitation dominated groundwater recharge at the Demnitzer Millcreek research catchment in Germany and thus was unlikely to dominate transpiration, which accounted for 70% of ET. types. Indeed, a meta-analysis has shown that winter precipitation dominates groundwater recharge in temperate climates

(Jasechko et al., 2014), but that does not rule out the possibility of that groundwater flux eventually contributing to ET, which recent research has suggested groundwater-to-ET flows to be more common than previously expected (Berghuijs et al., 2022).

Mostly importanlty, this study shows that long-term end-member-splitting results may not be consistent with precipitation partitioning in any given year. Although ET amounts did not systematically vary with seasonal precipitation variability (Figures S7J and S8J), the data suggested that contributions of each season's precipitation to ET were sensitive to seasonal precipitation amounts. Large statistical uncertainties limited confidently robustly rejecting our *a priori* hypothesis, that dry summers would result in greater fractions of winter precipitation being routed to ET to mitigate summer input deficits. Nonetheless, a more robust pattern was found in summer precipitation's contributions to ET increasing with dry winters. With greater winter precipitation inputs, more of that winter precipitation supplied ET, with contributions ranging from zero to >50 % of ET. Given that ET amounts were relatively consistent, summer precipitation contributions increased with drier winters and supplied the rest of ET (50 to 100 %). Summer precipitation amounts seem regularly sufficient to overwhelmingly displace stored winter precipitation from most or all of the storages that supply ET. However, we hypothesize that increasing winter precipitation contributions to ET in wetter winters may result from wetter winters yielding deeper snowpacks that enhance carryover of winter precipitation into the transpiration season or wetter soils that facilitate bypass flows by early summer precipitation (*sensu* Brooks et al., 2010). Thus, even if the winter

droughts observed in this record affected the sources used by ET in summer, we see no evidence to conclude that droughts in either season would reduce ET here, as might hypothetically occur if they resulted in plant stress (assuming transpiration contributions to ET are relatively consistent). These findings prompt the hypothesis that a dry summer following a dry winter might yield the critical conditions needed for watershed streamflow to be substantially increased because ET is drought-limited.

2.5 Reseach Chapter 1 References

Allen, S. T., von Freyberg, J., Weiler, M., Goldsmith, G. R., and Kirchner, J. W. (2019) The seasonal origins of streamwater in Switzerland. *Geophysical Research Letters, 46*(17-18), 10,425–10,434. https://doi.org/10.1029/2019GL084552

Arend, M., Link, R. M., Patthey, R., Hoch, G., Schuldt, B., and Kahmen, A. (2021) Rapid hydraulic collapse as cause of drought-induces mortality in conifers. *Proceedings of the National Academy of Sciences of the United States of America, 118*(16), 1-6. https://doi.org/10.1073/pnas.2025251118

Berghuijs, W. R., Luijendijk, E., Moeck, C., van der Velde, Y., and Allen, S. T. (2022). Global recharge data set indicates strengthened groundwater connection to surface fluxes. *Geophysical Research Letters, 49*(23), e2022GL099010. https://doi.org/10.1029/2022GL099010

Berkelhammer, M., Still, C. J., Ritter, F., Winnick, M., Anderson, L., Carroll, R., et al. (2020) Persistense and Plasticity in Conifer Water-Use Strategies. *Journal of Geophysical Research: Biogeosciences, 125*(2), e2018JG0004845. https://doi.org/10.1029/2018JG004845

Beven, K. and Germann, P. (1982) Macropores and Water Flow in Soils. *Water Resources Research, 18*(5), 1311-1325. https://doi.org/10.1029/WR018i005p01311

Brooks, J. R., Barnard, H. R., Coulombe, R., and McDonnell, J. J. (2010) Ecohydrologic separation of water between trees and streams in a Mediterranean climate. *Nature Geoscience, 3*, 100-104. https://doi.org/10.1038/ngeo722

Campbell, J. L. and Green, M. B. (2019) Water isotope samples from Watershed 3 at Hubbard Brook Experimental Forest, 2006-2010. https://doi.org/10.6073/pasta/f5740876b68ec42b695c39d8ad790cee

Ehleringer, J. R., Philips, S. L., Schuster, W. S. F., and Sandquist, D. R. (1991) Differential Utilization of Summer Rains by Desert Plants. *Oecologia, 88*(3), 430-434. https://www.jstor.org/stable/4219812

Goldsmith, G. R., Allen, S. T., Braun, S., Siegwolf, R. T. W., and Kirchner, J. W. (2022) Climatic Influences of Summer Use of Winter Precipitation by Trees. *Geophysical Research Letters, 49*(10), e2022GL098323. https://doi.org/10.1029/2022GL098323

Hirschi, M., Michel, D., Lehner, I., and Seneviratne, S. I. (2017) A site-level comparison of lysimeter and eddy covariance flux measurements of evapotranspiration. *Hydrology and Earth System Sciences, 21*(3), 1809-1825. https://doi.org/10.5194/hess-21-1809-2017

Jasechko, S., Birks, S. J., Gleeson, T., Wada, Y., Fawcett, P. J., Sharp, Z. D., et al. (2014), The pronounced seasonality of global groundwater recharge. *Water Resources Research, 50*(11), 8845–8867. https://doi.org/10.1002/ 2014WR015809

Kirchner, J. W., and Allen, S. T. (2020) Seasonal partitioning of precipitation between streamflow and evapotranspiration, inferred from end-member splitting analysis. *Hydrology and Earth System Sciences, 24*(1), 17-39. https://doi.org/10.5194/hess-24-17-2020

Kleine, L., Tetzlaff, D., Smith, A., Dubbert, M., and Soulsby, C. (2021) Modelling ecohydrological feedbacks in forest and grassland plots under a prolonged drought anomaly in Central Europe 2018-2020. *Hydrological Processes 35*(8), 1-20. https://doi.org/10.1002/hyp.14325

Lehner, I., Bernasconi, S., and Seneviratne, S. I. (2009) Mean water residence times in the pre-alpine Rietholzbach catchment. *EGU General Assembly Conference Abstracts*, 4744.

Lotsch, A., Friedl, M. A., Anderson, B. T., and Compton, J. T. (2005) Response of terrestrial ecosystems to recent Northern Hemispheric drought. *Geophysical Research Letters, 32*(6), 1-5. https://doi.org/10.1029/2004GL022043

Martin, J., Looker, N., Hoylman, Z., Jencso, K., and Hu, J. (2018). Differential use of winter precipitation by upper and lower elevation Douglas fir in the Northern Rockies. *Global change biology*, *24*(12), 5607-5621. https://doi.org/10.1111/gcb.14435

Michel, D. and Seneviratne, S. (2022) Multi-year eddy-covariance measurements at a pre-alpine humid grassland site: Dataset overview, drought responses, and effects of land management. *Agricultural and Forest Meteorology, 326*(2022), 109166. https://doi.org/10.1016/j.agrformet.2022.109166

Oertel, A. (2016) Hydrological and environmental signals in tree-ring $\delta^{18}O$ at the Rietholzbach catchment. Master's Thesis, Swiss Federal Institute of Technology Zurich.

Poage, M. A., and Chamberlain, C. P. (2001) Empirical relationships between elevation and the stable isotope composition of precipitation and surface waters: Considerations for studies of paleoelevation change. *American Journal of Science, 301*(1), 1-15. https://doi.org/10.2475/ajs.301.1.1

Schuldt, B., Buras, A., Arend, M., Vitasse, Y., Beierkuhnlein, C., Damm, A., et al. (2020) A first assessment of the impact of the extreme 2018 summer drought on Central European forests. *Basic and Applied Ecology, 45*, 86-103. https://doi.org/10.1016/j.baae.2020.04.003

Seneviratne, S. I., Lehner, I., Gurtz, J., Teuling, A. J., Lang, H., Moser, U., et al. (2012) Swiss prealpine Rietholzbach research catchment and lysimeter: 32 year time series and 2003 drought event. *Water Resources Research, 48*(6), 1-20. https://doi.org/10.1029/2011WR011749

Sprenger, M., Carroll, R. W. H., Dennedy-Frank, J., Siirila-Woodburn, E. R., Newcomer, M. E., Brown, W., et al. (2022a) Variability of snow and rainfall partitioning into evapotranspiration and summer runoff across nine mountainous catchments. *Geophysical Research Letters, 49*(13), e2022GL099324. https://doi.org/10.1029/2022GL099324

Sprenger, M., Llorens, P., Gallart, F., Benettin, P., Allen, S. T., and Latron, J. (2022b) Precipitation fate and transport in a Mediterranean catchment through models calibrated on plant and stream water isotope data. *Hydrology and Earth System Sciences, 26*, 4093-4107. https://doi.org/10.5194/hess-26-4093-2022

Teuling, A. J., Lehner, I., Kirchner, J. W., and Seneviratne, S. I. (2010) Catchments as simple dynamical systems: Experience from a Swiss prealpine catchment. *Water Resources Research, 46*(10), 1-15. https://doi.org/10.1029/2009WR008777

Van Rossum, G., and Drake Jr, F. L. (2009) *Python 3 Reference Manual*. Scotts Valley, CA: CreateSpace.

Vitvar, T. and Balderer, W. (1997) Estimation of mean water residence times and runoff generation by ^{18}O measurements in a Pre-Alpine catchment (Ritholzbach, Eastern Switzerland). *Applied Geochemistry, 12*(6), 787-796. https://doi.org/10.1016/S0883-2927(97)00045-0

von Freyberg, J., Allen, S. T., Seeger, S., Weiler, M., and Kirchner, J. W. (2018) Sensitivity of young water fractions to hydro-climatic forcing and landscape properties across

22 Swiss catchments. *Hydrology and Earth System Sciences, 22*(7), 3841–3861, https://doi.org/10.5194/hess-22-3841-2018

von Freyberg, J., Rao, P. S. C., Radny, D., Schirmer, M. (2015) The impact of hillslope groundwater dynamics and landscape functioning in event-flow generation: a field study in the Rietholzbach catchment, Switzerland. *Hydrogeology Journal 23*(5), 935-948. https://doi.org/ 10.1007/s10040-015-1238-1

3. Research Chapter 2. Landscape-level controls over the partitioning of seasonal precipitation into evapotranspiration

3.1. Introduction

Several studies have identified long-term trends in seasonal precipitation amount across the U.S. (Vose et al., 2014; Martino et al., 2013). To predict how these ongoing changes will affect water resources, we must understand how seasonal precipitation inputs are partitioned between runoff and evapotranspiration (ET). Vegetation could be dependent on precipitation from a single season and, therefore, especially vulnerable to droughts occurring during that season. For example, grasslands and aridlands respond to summer precipitation pulses (Patrick et al., 2007; Feldman et al., 2021) while forests can tap into deep water sources that can sustain them in the absence of precipitation (Liu et al., 2019; McCormick et al., 2021). It is commonly believed that summer precipitation recharges soil water deficits because soil water deficits mostly occur during summer when ET is high. The remainder of precipitation supplies streamflow. If summer precipitation supplies streamflow even in environments where soil water deficits occur, this would challenge our basic assumptions about how soil water recharge occurs (Brunke et al., 2016).

We can calculate this partitioning using long-term timeseries of precipitation and runoff isotopes and flux amounts through end-member mixing and end-member splitting analyses (Kirchner and Allen, 2020). The end-member splitting method goes beyond end-member mixing (which addresses the relative fraction of each end-member in a mixture) by also making use of mass-flux data to address how each end-member is

partitioned among its different fates. In the case of this study, the two input end members are summer (April – September) and winter (October – March) precipitation and the measured mixture is annual runoff. This method assumes that all inputs to runoff are accounted for and that there are no changes in watershed storage. To meet these assumptions, end-member mixing and splitting are typically done using multiple years of data (Kirchner and Allen, 2020).

New opportunities are presented by the measurements of the National Ecological Observatory Network (NEON). Across the contiguous U.S., there are 34 NEON aquatic sites that were selected to represent different systems within the United States, thus spanning a diversity of topographies, climates, and ecosystems (NEON, 2022a). Stable isotopes ratios of water, $\delta^{2}H$ and $\delta^{18}O$, are among the numerous metrics characterized for routinely collected water samples. Such a dataset provides new opportunities to compare the fates of precipitation across diverse landscapes through end-member splitting analyses. Moreover, we can use the diverse NEON sites to explore relationships between site characteristics and partitioning fractions using continuous geospatial datasets.

The objectives of this study are to 1) calculate precipitation routing for the NEON sites and 2) identify relationships between partitioning fractions and watershed-scale landscape and climate characteristics inferred from geospatial datasets. We hypothesize that the fraction of summer precipitation supplying ET and the fraction of ET supplied by summer precipitation will both vary tremendously across the U.S., and that remotely sensed vegetation characteristics will correlate with those partitioning fractions.

Specifically, we hypothesize that ET will be largely sourced from summer precipitation in landscapes where vegetation functioning is more dynamic because ecosystems without access to stored winter precipitation are more likely to be affected by summer droughts; that dynamism which will be captured by quantifying the stability of values of various metrics that capture vegetation vigor.

3.2. Methods

First, we'll briefly describe the sources of the data used in this project. Section 3.2.2 details how we subset the NEON data and conducted end-member splitting. This section also contains a table showing details about each NEON site. Section 3.2.3 describes geospatial data processing. Section 3.2.4 explains how we built exploratory models of partitioning using watershed-level summaries of the geospatial datasets.

3.2.1. Data Sources

Streamflow isotope and runoff data were obtained from a subset of the NEON database, along with watershed boundary files (NEON, 2022b; NEON, 2022c). Subsetting of NEON sites is explained in section 3.2.2. We also used a previously developed continuous runoff data product derived from NEON data (Rhea, 2023). The data extend from December 2014 to present. A continuous dataset of biweekly samples was the target, but logistical impediments (including responses to the covid-19 pandemic) resulted in gaps and uneven sampling at times; the final dataset used by us is described in the following section.

Monthly grids of hydrogen isotope ratios (δ^2H) in precipitation were downloaded from the Water Isotope Database (Bowen, 2022; Bowen et al., 2005). These grids cover the contiguous U.S. at 1-km resolution. Monthly grids of average precipitation amount (1991-2020) were obtained at 800-m resolution (PRISM Climate Group, 2014). Elevation data were downloaded as a 1 arc-second (approximately 30 m) grid (U.S. Geological Survey, 2019). Vegetation indices were calculated from two Moderate Resolution Imaging Spectroradiometer (MODIS) products: MCD19A1 Multi-Angle Implementation of Atmospheric Correction Land Surface Bidirectional Reflectance Factor (Lyapustin and Wang, 2018) and MCD12Q2 Yearly Land Cover Dynamics (Friedl et al., 2019). We downloaded 1-km MCD19A1 imagery collected from April 1 to September 30, 2018, overlapping with the times when stable isotopes sample were collected at most of the sites. The 500-m MCD12Q2 data used in this study was also from 2018, but unlike the MCD19A1 product, it integrates information from imagery collected throughout the entire year. To estimate canopy height, we used a 30-m fusion product using GEDI (~30-m GSD, unevenly sampled) and 30-m GSD wall-to-wall Landsat data (Potapov et al., 2020).

3.2.2. Isotope Data Processing

We removed all sites from the NEON watersheds dataset which were located outside of the contiguous U.S. Sites further south than 30 degrees N were also removed because southern sites have a dampened seasonal precipitation isotope signal (Bowen, 2008) and the analyses in this paper depend on the ability to differentiate summer

precipitation from winter precipitation. Furthermore, the removed southern sites are in hurricane zones and hurricanes have abnormal precipitation isotope signatures which could further confound the seasonal signal (Sanchez-Murillo et al., 2019). Lake sites were also removed because they did not have runoff data which is needed for end-member splitting, and they were likely to demonstrate strong evaporative fractionation signals that would also bias results. Details of the remaining data from 23 sites are available in Table 3.1.

Table 3.1. Summary of NEON site characteristics including state, watershed area, mean annual temperature, mean annual precipitation, the start of runoff isotope sampling (mm-yy), the number of runoff isotope measurements, the hydrogen isotope ratio (‰) of runoff, the hydrogen isotope ratio (‰) of summer precipitation (P_S), the hydrogen isotope ratio (‰) of winter precipitation (P_W), the fraction of summer precipitation routed to ET ± standard error, and the fraction of ET sourced from summer precipitation ± standard error.

NEON Site & State	Area (km^2)	Temp (°C)	Ppt. (mm)	Start Month	No. Points	Runoff δ^2H (‰)	P_S δ^2H (‰)	P_W δ^2H (‰)	Fraction of P_S to ET	Fraction of ET from P_S
MCRA, OR	3.9	7.8	2240	06-17	92	-75.0	-65.3	-88.4	-0.72 ± 0.41	-0.63 ± 0.34
MART, WA	6.3	8.9	2640	11-17	101	-70.1	-62.2	-83.0	-0.63 ± 0.37	-0.24 ± 0.14
TECR, CA	3.0	8.5	1150	10-18	49	-86.0	-66.4	-104.2	-0.31 ± 0.22	-0.07 ± 0.05
BIGC, CA	11	12.4	910	02-18	70	-80.2	-64.8	-94.6	0.23 ± 0.16	0.04 ± 0.03
BLWA, AL	16000	16.8	1480	10-16	121	-21.9	-20.6	-28.6	013 ± 0.16	0.11 ± 0.13
FLNT, GA	15000	18.0	1280	03-17	86	-20.5	-21.2	-28.5	0.31 ± 0.12	0.21 ± 0.08
MAYF, AL	14	17.5	1410	03-15	149	-20.8	-19.5	-24.9	0.31 ± 0.16	0.23 ± 0.12
TOMB, AL	47000	17.0	1480	10-16	111	-21.9	-19.8	-27.6	0.31 ± 0.17	0.24 ± 0.13
SYCA, AZ	280	16.7	510	06-17	64	-69.8	-39.7	-66.4	1.01 ± 0.11	0.36 ± 0.03
REDB, UT	17	7.1	820	10-16	108	-123.3	-84.0	-128.0	0.95 ± 0.12	0.40 ± 0.04
WALK, TN	1.1	12.8	1440	11-15	143	-36.2	-26.6	-44.8	0.52 ± 0.12	0.43 ± 0.08
HOPB, MA	12	7.7	1320	09-16	123	-54.5	-42.2	-74.3	0.51 ± 0.11	0.47 ± 0.09
COMO, CO	3.6	0.7	940	08-15	142	-131.4	-72.3	-142.4	0.86 ± 0.14	0.55 ± 0.07
BLUE, OK	320	16.0	1060	01-17	89	-28.8	-24.2	-41.1	0.72 ± 0.10	0.56 ± 0.06
POSE, VA	2.0	12.0	1130	12-14	166	-46.9	-35.0	-62.1	0.69 ± 0.11	0.56 ± 0.07
PRIN, TX	49	17.5	880	08-16	104	-25.1	-23.2	-34.5	0.88 ± 0.11	0.56 ± 0.05
LEWI, VA	12	12.4	1030	10-16	124	-48.9	-33.5	-59.4	0.87 ± 0.11	0.60 ± 0.06
BLDE, WY	38	2.1	580	03-18	77	-143.7	-86.2	-150.5	0.94 ± 0.13	0.64 ± 0.07
LECO, TN	9.1	11.2	1810	02-16	127	-44.2	-25.4	-51.8	0.77 ± 0.13	0.65 ± 0.08
MCDI, KS	23	12.4	920	09-16	109	-37.6	-31.6	-68.0	0.86 ± 0.11	0.68 ± 0.06
KING, KS	13	12.7	870	10-15	134	-40.1	-31.6	-68.1	0.83 ± 0.11	0.69 ± 0.07
ARIK, CO	2600	7.7	430	06-15	127	-75.8	-58.6	-107.4	1.00 ± 0.11	0.76 ± 0.06
WLOU, CO	4.9	1.9	680	05-17	111	-130.9	-62.5	-128.0	1.06 ± 0.22	1.11 ± 0.17

For the remaining 23 sites, we calculated weighted mean isotope signatures and flux amounts for annual runoff and seasonal precipitation. For runoff isotope signatures, samples were assigned weights using the Rhea (2023) dataset of modeled continuous runoff and equation 1 where Q_i is daily runoff rate for days when samples were collected for isotope analysis within each month, Q_M is average monthly runoff rate for each month, and N is the number of isotope samples collected in the given month.

$$\text{Weight}_i = \left(1 + \frac{(Q_i - Q_M)}{Q_M}\right) \frac{Q_M}{N} \quad (3.1)$$

This equation calculates a proportional weight relative to mean monthly runoff and ensures that months with more frequent sampling are not overrepresented in calculations of annual runoff isotopes. For runoff amounts, we summed the monthly averages of the field measurements downloaded directly from NEON.

For precipitation isotope signatures, we first used bilinear interpolation to rescale the 800-m amount grids to align with the 1-km isotope grids and then multiplied the two rasters. The product was used to calculate a spatially weighted isotope signature at each site for each month. Because these coarse-scale calculations could misrepresent elevation and precipitation isotope ratios depend on elevation, an elevation correction was added using the difference between the mean watershed elevation calculated from a 1 km DEM and the mean watershed elevation calculated from a 10 m DEM; that difference was multiplied by 0.0224 ‰ δ^2H m^{-1}, a previously reported precipitation isolate lapse rate, to adjust for elevation discrepancies (Poage and Chamberlain, 2001). Seasonal precipitation isotope signatures were calculated as a

weighted mean of data from April through September for the summer and from October through March for winter. For precipitation amounts, we summed the spatial averages of the monthly precipitation grids. We then conducted end-member mixing and splitting analyses to estimate the fraction of summer precipitation routed to ET and the fraction of ET sourced from summer precipitation as described in section 2.2.1. Standard errors were calculated with gaussian error propagation. Since no uncertainty grids were provided with the precipitation amount grids, we used a conservative estimate of the standard error being 5.5 % of precipitation amounts (Daly et al., 2008).

3.2.3. Geospatial Data Processing

To explore physiographic factors' relationship with end-member-splitting products, geospatial data were processed to calculate an average value for each product at each site. MODIS products were averaged and aggregated spatially and temporally. The MCD12Q2 product provided Enhanced Vegetation Indices (EVI) summary rasters including values of minimum, amplitude, and area under the growing season curve. Those data, in addition to forest canopy height (Potapov et al, 2020), total annual precipitation (PRISM Climate Group, 2014), and the ratio of summer precipitation to annual precipitation (PRISM Climate Group, 2014) were spatially averaged to yield a watershed-mean value for every image. For the MCD19A1 product used to calculate the chlorophyll carotenoid index (CCI), the data were first temporally averaged for each month, and then the median monthly values within each watershed were used to calculate the coefficient of variation, standard deviation, minimum, and the difference

between peak-season and late-season CCI. Data processing was completed using Python 3.9 in PyCharm2021.2.1 (Van Rossum and Drake, 2009) and using ArcGIS Pro (Esri, 2021).

3.2.3. Analysis

First, watershed-averaged site characteristics (coefficient of variation of CCI, standard deviation of CCI, difference between peak and late-season CCI, peak CCI, minimum CCI, the ratio of summer precipitation to annual precipitation, mean annual precipitation, forest height, EVI amplitude, EVI area-under-the-curve, and EVI minimum) were tested for correlations with each of the key end-member splitting metrics focused on here: the fraction of ET from summer precipitation and the fraction of summer precipitation supplying ET. To explore a multi-variate model space, a stepwise regression was used to select predictors from the set of variables included above. An inverse-error-weighted regression-model fit was used to down-weight the influence of the poorly constrained points (which were also outliers with implausible values); variables were added and removed to minimize BIC to select a final model. We did not use interaction terms because overfitting was likely with the high number of potential predictors and the low number of samples. We encountered issues related to overfitting even with the routine used, but they are interpreted accordingly, and this risk is justified by our motivation being to explore potential explanatory variables, rather than to develop a predictive model. Model building and fitting was done in MATLAB (The MathWorks inc., 2022). In Python, we conducted leave-one-out cross-validation to calculate mean absolute error (MAE) and root mean square error (RMSE).

3.3. Results

Both fractions of ET from summer precipitation and fractions of summer precipitation supplying ET spanned the entire 0-to-1 range of plausible values, with outliers extending outside of this range (Table 3.1; Figure 3.1). The two end-member-splitting products show distinct regional patterns, with sites in Pacific-Coast states and Gulf states similarly showing smaller fluxes of summer precipitation to ET and small fractions of ET coming from summer precipitation. Sites in the central U.S. and the northeast tend to show a larger relative flux of summer precipitation to ET, and a relatively larger fraction of ET sourced from summer precipitation. More mixed values occurred in the southern plains (sites BLUE and PRIN) where there were intermediate fractions of ET from summer and winter precipitation, which involved a majority of summer precipitation contributing to ET. A similar pattern was seen for many of the inter-mountain west sites, especially towards the ones in hotter and drier climates (REDB and SYCA).

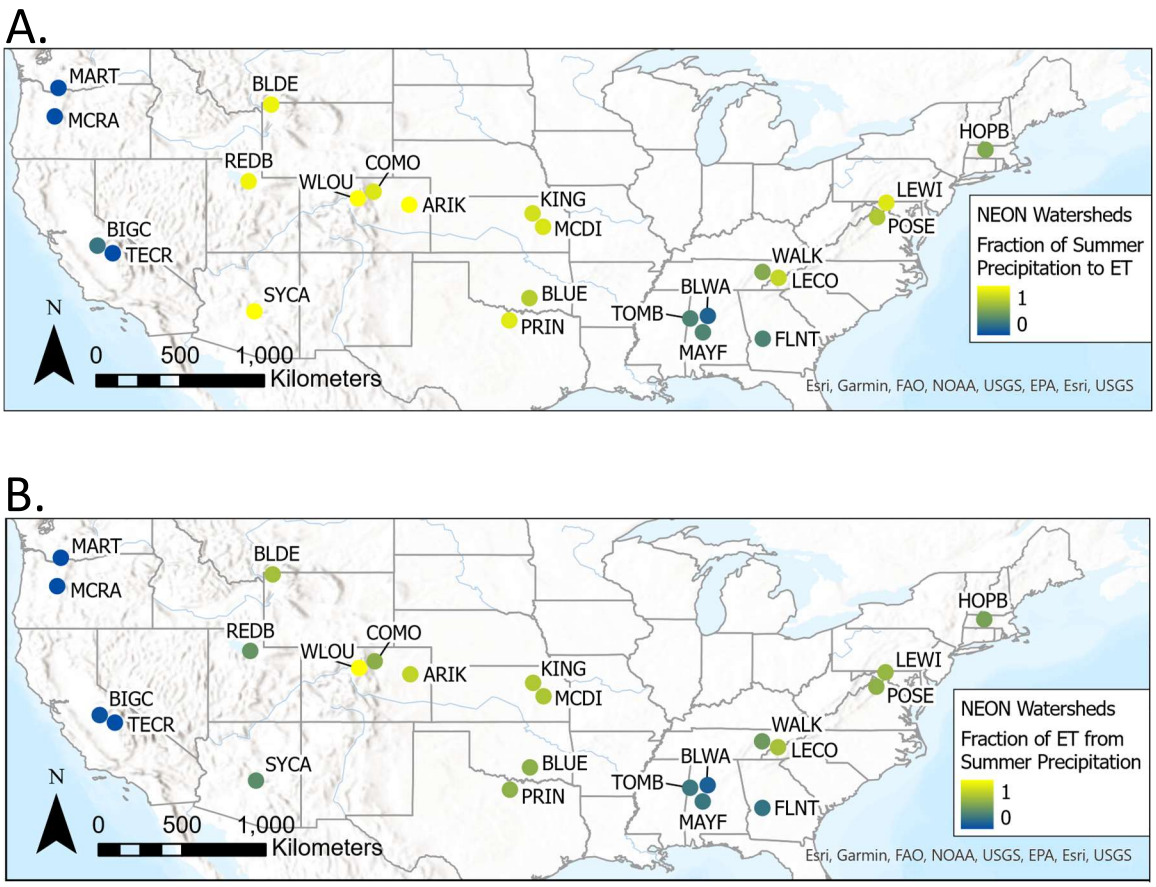

Figure 3.1. Map of all 23 watersheds showing the fraction of summer precipitation routed to ET (A) and the fraction of ET sourced from summer precipitation (B). The two metrics appear to be correlated and seem to show regional similarities. Sites near the west coast of the U.S. or the Gulf of Mexico tend to have a smaller relative flux from summer precipitation to ET. Sites closer to the central U.S. or the northeast tend to have a larger relative flux from summer precipitation to ET.

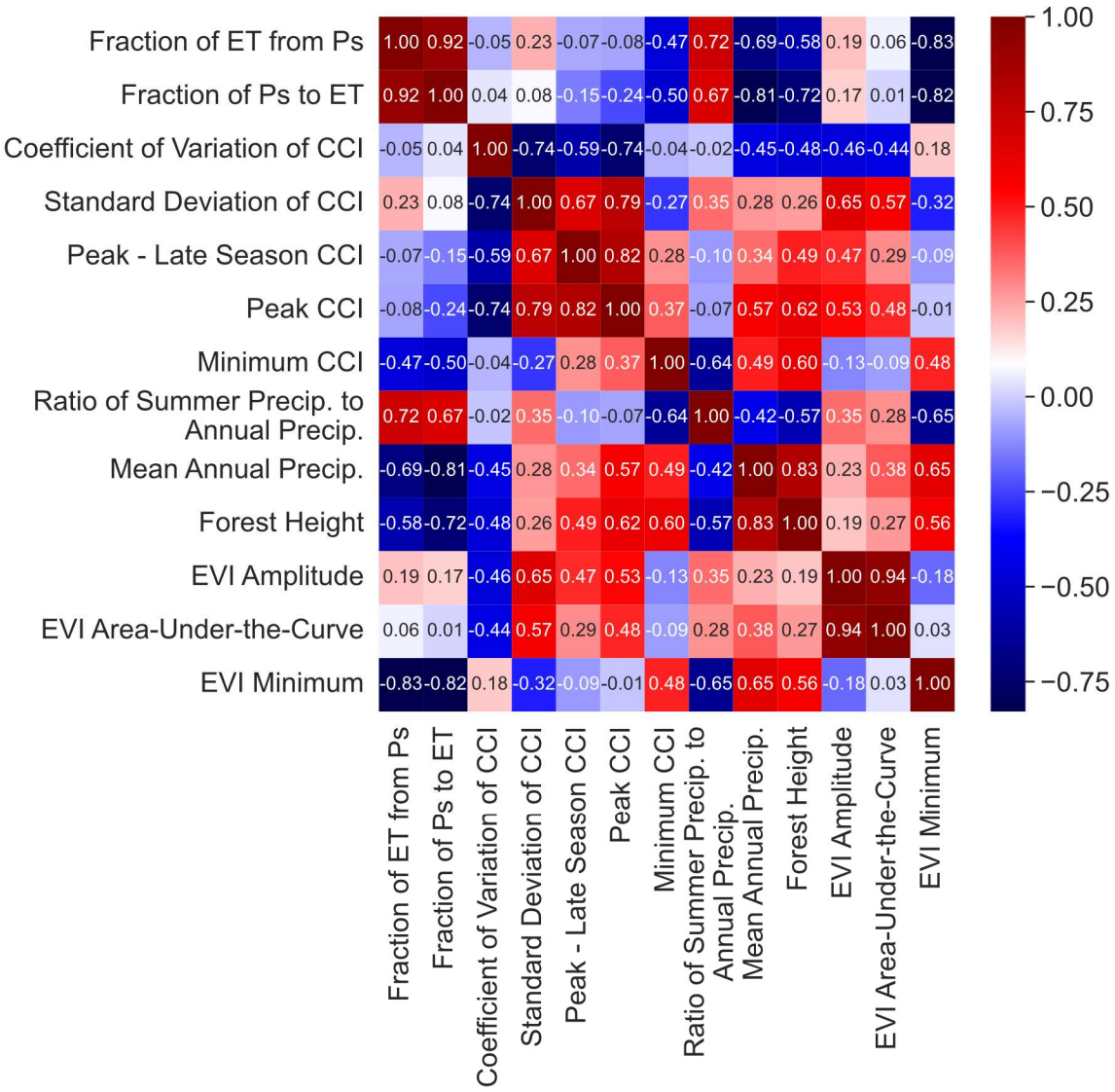

Figure 3.2. Correlation matrix showing the Pearson correlation coefficients between the fraction of summer precipitation (Ps) to evapotranspiration (ET), the fraction of ET from Ps, and the full list of potential predictive variables assessed in this analysis. Light colors represent weak relationships while dark red represents positive correlations and dark blue represents negative correlations. Many of the potential predictive variables are correlated with each other.

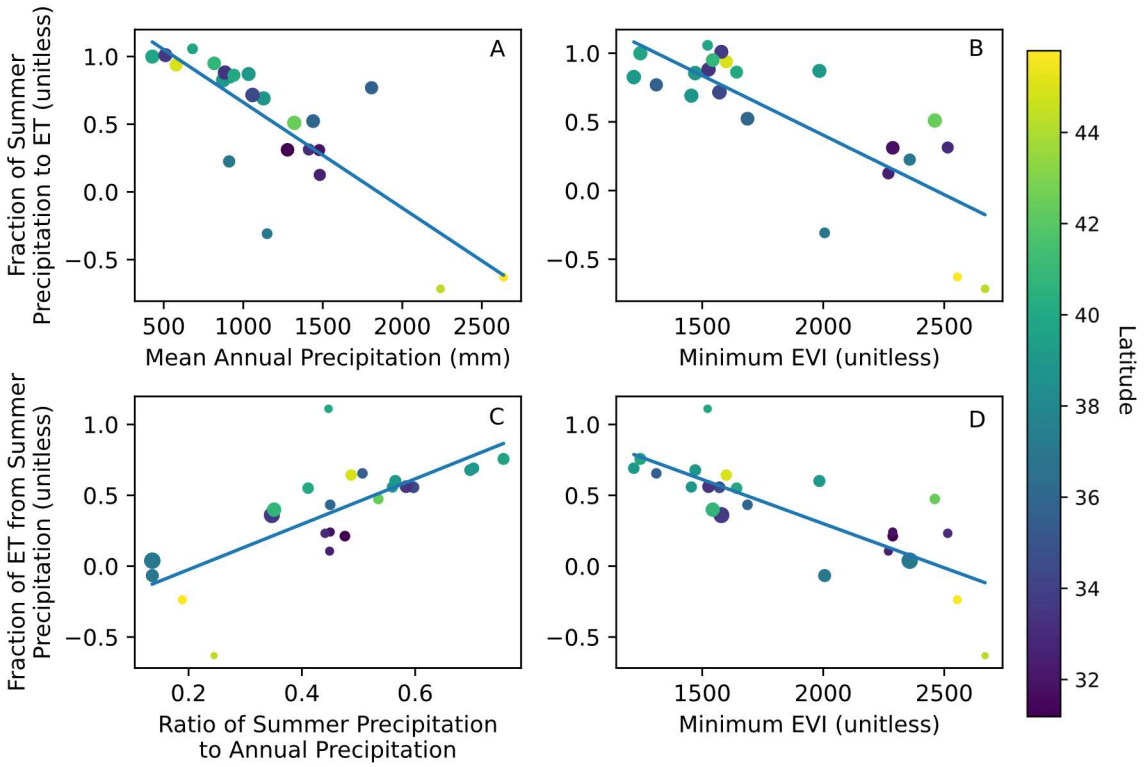

Figure 3.3. Scatter plots of key site characteristics against the fraction of summer precipitation to ET and the fraction of ET from summer precipitation with ordinary least-squares regression trendlines. The color of each point represents the latitude of the site. Of the 11 potential predictive variables tested, the fraction of summer precipitation to ET was most correlated with mean annual precipitation (Panel A, R^2=0.65) and minimum EVI (Panel B, R^2=0.63). The fraction of ET from summer precipitation was most correlated with minimum EVI (Panel D, R^2=0.61) and the ratio of summer precipitation to annual precipitation (Panel C, R^2=0.52).

Figure 3.3 shows the two variables with the strongest regression fits (R^2) for each target. Mean annual precipitation was the best correlate of the fraction of summer precipitation to ET (R^2=.65). Minimum EVI was also highly correlated with the target (R^2=.63), but somewhat redundant with mean annual precipitation (R^2=.42). For the fraction of ET from summer precipitation, the ratio of summer precipitation to annual precipitation was a strong correlate (R^2=.52) with a slope of 1.6 (p<.001); A 1:1 relationship between these variables would indicate no bias in the use of seasonal precipitation for ET. Minimum EVI was more correlated with the target (R^2=.69) ratio of

summer precipitation to annual precipitation, but it was also redundant with the ratio of summer precipitation to annual precipitation (R^2=.42) and thus less important in the multi-variate model. The multivariate model fitting optimized BIC while testing all linear combinations to yield a 4-variable model for the fraction of summer precipitation routed to ET, composed of negative coefficients for the coefficient of variation of CCI (p=.07), mean annual precipitation (p<.001), and minimum EVI (p=.12) and a positive coefficient for EVI area-under-the-curve (p=.02). The adjusted R^2 value of this model was 0.79 (p<.001). From leave-one-out cross-validation, the MAE was 0.16 and the RMSE was 0.22 (Figure 3.3). Optimizing BIC while fitting all linear combinations yielded a 2-variable model for the fraction of ET from summer precipitation which included a positive influence of the ratio of summer precipitation to annual precipitation (p<.001) and a negative influence of minimum EVI (p=.005). The adjusted R^2 value of this model was 0.76 (p<.001). From leave-one-out cross-validation, the MAE was 0.15 and the RMSE was 0.22 (Figure 3.4).

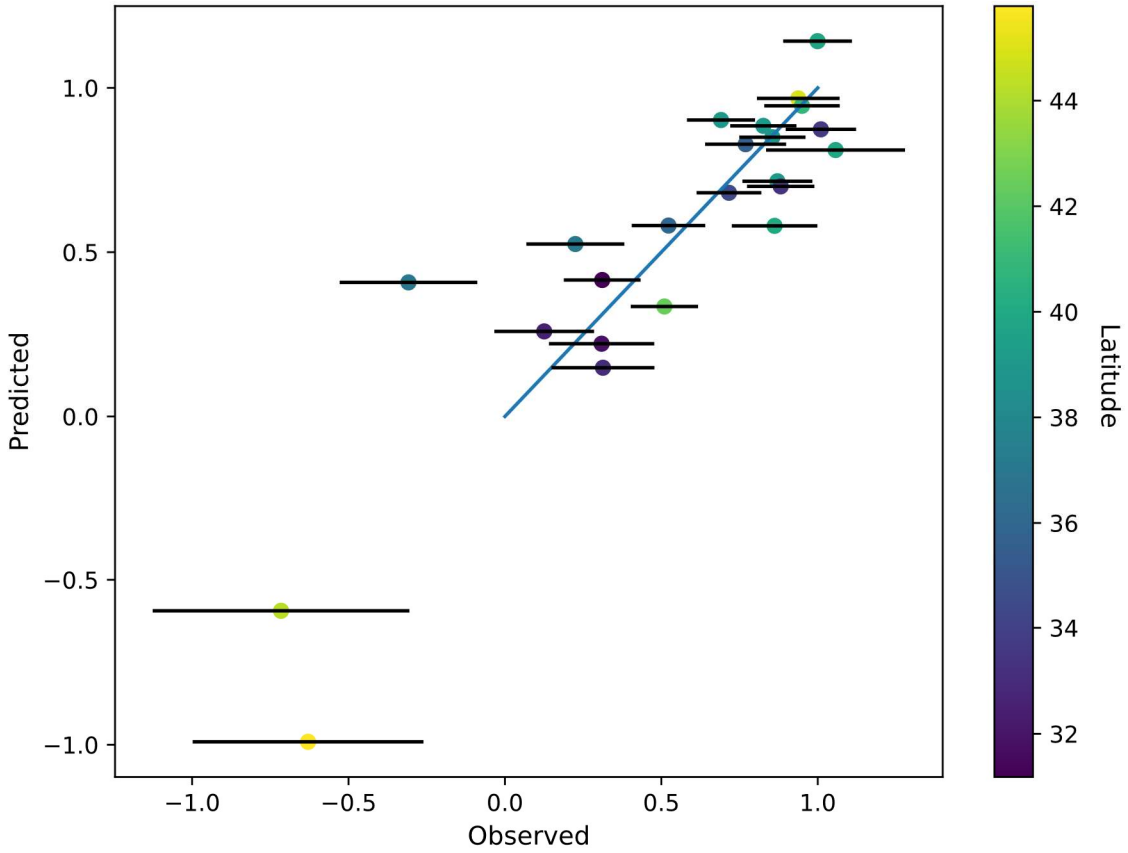

Figure 3.4. Observed versus predicted values of the fraction of summer precipitation to ET with observed standard error. The color of each point represents the latitude of the site. Predictions were made using a weighted least squares regression trained on all data except the point being predicted. A 1:1 line is plotted over the range of 0 to 1 to show the bounds of reasonable values for the fraction of summer precipitation to ET. The points that fall outside this range appear to have the greatest observed error and all are within 2 standard errors of the range of reasonable values.

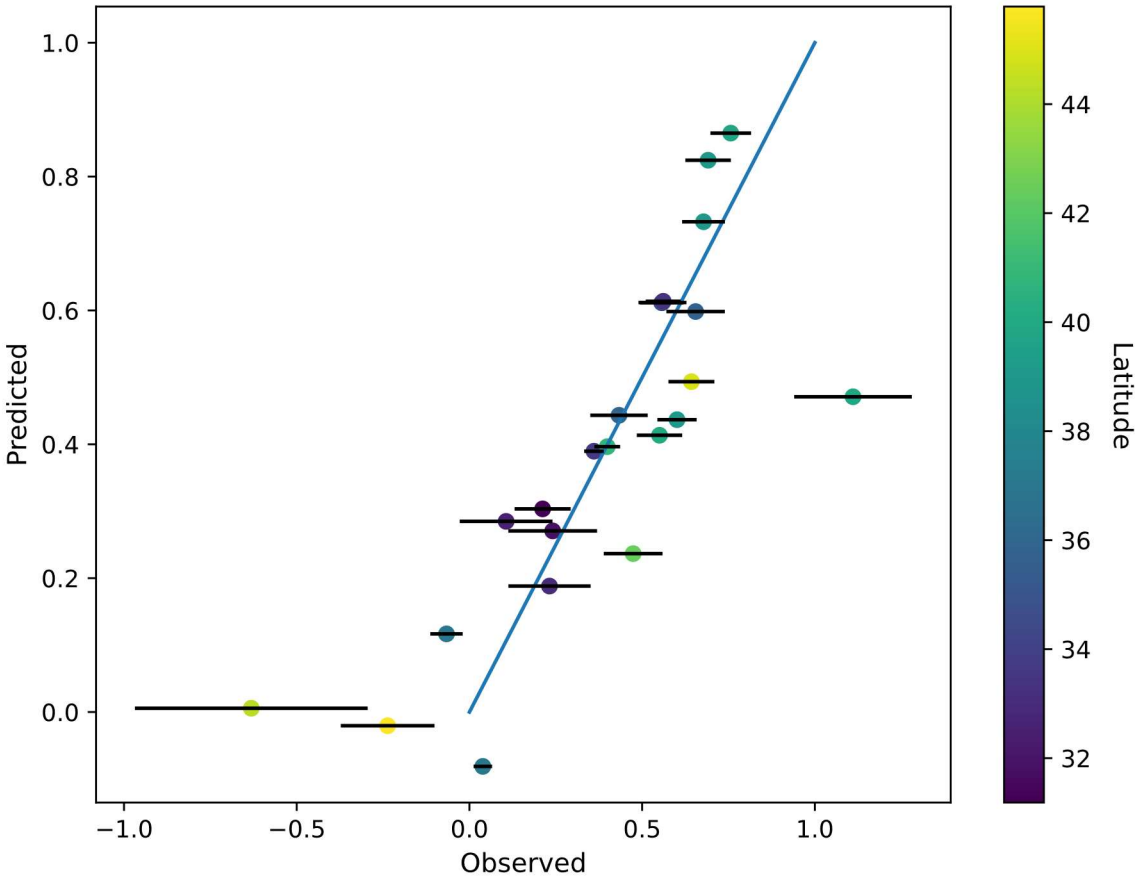

Figure 3.5. Observed versus predicted values of the fraction of ET from summer precipitation with observed standard error. The color of each point represents the latitude of the site. Predictions were made using a weighted least squares regression trained on all data except the point being predicted. A 1:1 line is plotted over the range of 0 to 1 to show the bounds of reasonable values for the fraction of ET from summer precipitation. The points that fall outside this range appear to have the greatest observed error and all are within 2 standard errors of the range of reasonable values.

3.4. Discussion

Our calculations of the fraction of summer precipitation to ET and the fraction of ET from summer precipitation show that precipitation partitioning is highly variable across the contiguous U.S. The average standard error of partitioning calculations was low at 0.16 for the fraction of summer precipitation to runoff and 0.09 for the fraction of ET from summer precipitation, so we can robustly distinguish between high and low values. Smaller fluxes of summer precipitation to ET and small fractions of ET coming

from summer precipitation were seen in both the Pacific west and the Gulf-of-Mexico states, despite the strong contrasts between those regions' climates. The Pacific west ranges substantially in total annual precipitation, but has most precipitation falling in winter, in contrast with the Gulf region where rainfall occurs fall year-round. However, the result is not surprising given that these regions can have forests with high productivity, even in winter because they have mild winters and some evergreen cover. Thus, a substantial fraction of ET may occur in winter in the Pacific west and the Gulf region (Liu et al., 2017). Moreover, summer precipitation in the southeast involves frequent high-intensity precipitation that is more likely to quickly run off surfaces rather than infiltrate and recharge storages that supply vegetation. That said, it should also be noted that these sites are also ones where end-member-splitting is less ideal, due to either the small range between summer and winter precipitation isotope ratios or the small amounts of precipitation falling in summer.

The Mountain West and Southern Great Plains tend to have intermediate fractions of ET from summer and winter precipitation, which involved a majority of summer precipitation contributing to ET. These partitioning fractions may suggest that these ecosystems have the capacity to resist summer droughts because vegetation there can seemingly access winter precipitation and supplement limited summer precipitation sources with winter precipitation. However, this study does not resolve the relative importance of that summer precipitation and thus does not imply the consequences of summer droughts on ET (and vegetation health).

To discuss and interpret the implications of high-versus-low partitioning fractions throughout the rest of the U.S., we assume that most ET occurs during summer when vegetation is usually most photosynthetically active. The Central U.S. and the Northeast tend to show a larger relative flux of summer precipitation to ET, and a relatively larger fraction of ET sourced from summer precipitation. This high fraction of ET from summer precipitation suggests that vegetation is only able to access recent precipitation which may cause an ecosystem to be vulnerable to drought. With the high fraction of summer precipitation to ET, this might mean that even a small decrease in summer precipitation would limit ET and increase vegetation water stress. These regions tend to have sufficient precipitation in summer to supply ET, which is not expected to drive plants to establish deep roots (Fan et al., 2017), thereby make vegetation less likely to be able to tap into deeper water sources composed by larger fractions of winter precipitation.

The stepwise regression models and correlations between partitioning fractions and site characteristics show that variations in the fraction of summer precipitation to ET and the fraction of ET from summer precipitation are a function of climate and vegetation characteristics. Both mean annual precipitation (R^2=0.65) and minimum EVI (R^2=0.63) were independently strong predictors of the fraction of summer precipitation to ET, suggesting that both vegetation and climate may be a first-order drivers of that partitioning. Of course, it should be noted that the amount of summer precipitation among these sites probably has a substantially larger range than that of ET, and thus it makes sense that smaller fractions of larger amounts of summer precipitation would be needed to supply ET in regions with wet summers. While the coefficient of variation of

CCI and the EVI area-under-the-curve were chosen in the model of the fraction of summer precipitation to ET, these variables were not independently correlated with the target (R^2=.0016 and R^2=.0001, respectively). For the fraction of ET from summer precipitation, the ratio of summer precipitation to annual precipitation was a strong correlate (R^2=.52), and the slope of the relationship suggests that variations in fractions of precipitation falling in winter corresponds with variations in fraction of ET from winter. Minimum EVI covaried more strongly with the target variable (R^2=.69) but likely was less important in the multi-variate model because the minimum EVI distribution is bimodal, potentially representing seasonal ET trends in evergreen versus deciduous systems (Liu et al., 2017). We would expect deciduous systems to have a lower minimum EVI and to be more biased toward the use of summer precipitation since they are dormant in the winter.

While this is the first study using end-member splitting across a range of climates, our results can be compared to others' findings. At the Hubbard Brook Experimental Forest in New Hampshire, which has deciduous vegetation and 1360 mm of precipitation annually distributed relatively evenly throughout the year, the fraction of summer precipitation to ET was 0.44 ± 0.08 and the fraction of ET from summer was 0.85 ± 0.15 (Kirchner and Allen, 2020); this coheres with our findings in section 3. At the Rietholzbach watershed in northeastern Switzerland, which has mostly grassland cover and 1450 mm of precipitation annually with more precipitation falling during the summer, the fraction of summer precipitation to ET was 0.64 ± 0.09 and the fraction of ET from summer was 1.01 ± 0.16. Using remote sensing analyses, Feldman et al. (2021)

found that in arid regions, vegetation water content increases over multiple days following precipitation pulses, facilitating production and photosynthesis. This could lead to the expectation that arid ecosystems utilize a greater proportion of recent summer precipitation than mesic systems, which may be consistent with the relationship identified in Figure 3.3A. However, true arid systems are not ideal for end-member splitting because a) runoff fractions are often minimal and b) short-lived pulses may reflect quick uses of precipitation by plants but a lack of plant response could still involve that precipitation evaporating from soils and thereby contributing to ET fluxes. Huxman et al. (2004) found that rain use efficiency decreases across ecosystems as mean annual precipitation increases, consistent with our finding that less summer precipitation contributes to ET as annual precipitation increases (Figure 3.3A). Goodwell et al. (2018) found that precipitation pulses which increase ET and connectivity between ET and atmospheric and soil variables were most identifiable at the driest sites they studied, suggesting that drier sites may be more responsive to summer precipitation. Our results may not agree with those of Reynolds et al. (2004), which modeled plant productivity in extremely dry sites and argued that productivity was often greatest during the winter due to higher soil water availability (which presumably involved that productivity occurring with increasing ET of recent precipitation); however, we did not study any comparable systems since our driest site had at least 200 mm greater mean annual precipitation than the sites used in the study by Reynolds et al. Thus, while new metrics and insights are presented in our study, the arguments they support are largely

complementary to prior findings, adding another dimension of understanding of regional differences in controls over water use.

3.5 Conclusions

This research shows characterizable geospatial patterns and strong relationships of end-member-splitting results with site characteristics. These initial results can guide future efforts to build a predictive model of precipitation partitioning across the contiguous U.S. The results of leave-one-out cross-validation suggest that partitioning fractions could be predicted with MAE below 0.2 and RMSE below 0.25, but we would need a true separation of training and testing data to accurately assess the predictive power of a model. This separation would likely reduce the model fit. Such models could help land managers assess the vulnerability of water resources and terrestrial ecosystems to changes in seasonal precipitation. Characterizing precipitation partitioning also helps us understand how waters mix and recharge different hydrologic storages (e.g., surface soils vs. aquifers) that ultimately serve distinct functions (e.g., supporting plants vs. supplying rivers).

3.6 References for Research Chapter 2

Bowen, G. J. (2008) Spatial analysis of the intra-annual variation of precipitation isotope ratios and its climatological corollaries. *Journal of Geophysical Research: Atmospheres, 113*(D5). https://doi.org/10.1029/2007JD009295.

Bowen, G. J. (2022) Gridded maps of the isotopic composition of meteoric waters. http://www.waterisotopes.org.

Bowen G. J., Wassenaar, L. I., and Hobson, K. A. (2005) Global application of stable hydrogen and oxygen isotopes to wildlife forensics. *Oecologia, 143*, 337-348. https://doi.org/10.1007/s00442-004-1813-y.

Brunke, M. A., Broxton, P., Pelletier, J., Gochis, D., Hazenberg, P., Lawrence, D. M. et al. (2016) Implementing and Evaluating Variable Soil Thickness in the Community Land Model, Version 4.5 (CLM4.5). *Journal of Climate, 29*(9), 3441-3461. https://doi.org/10.1175/JCLI-D-15-0307.1

Daly, C., M. Halbleib, J.I. Smith, W.P. Gibson, M.K. Doggett, G.H. Taylor, et al. (2008) Physiographically-sensitive mapping of temperature and precipitation across the conterminous United States. *International Journal of Climatology 28*(15): 2031-2064. https://doi.org/10.1002/joc.1688.

Esri (2021) ArcGIS Pro. Version 2.8.0. Redlands, CA: Environmental Systems Research Institute, Inc.

Fan, Y., Miguez-Macho, G., Jobbágy, E. G., Jackson, R. B., and Otero-Casal, C. (2017). Hydrologic regulation of plant rooting depth. *Proceedings of the National Academy of Sciences, 114*(40), 10572-10577. https://doi.org/10.1073/pnas.1712381114.

Feldman, A. F., Gianotti, D. J. S., Koning, A. G., Gentine, P., and Entekhabi, D. (2021) Patterns of plant rehydration and growth pulses of soil moisture availability. *Biogeosciences, 18*(3), 831-847. https://doi.org/10.5194/bg-18-831-2021.

Friedl, M., Gray, J., Sulla-Menashe, D. (2019). MCD12Q2 MODIS/Terra+Aqua Land Cover Dynamics Yearly L3 Global 500m SIN Grid V006. NASA EOSDIS Land Processes DAAC. Accessed 2023-04-12 from https://doi.org/10.5067/MODIS/MCD12Q2.006.

Goodwell, A., Kumar, P., Fellows, A. W., and Flerchinger, G. N. (2018) Dynamic process connectivity explains ecohydrologic responses to rainfall pulses and drought. *Proceedings of the National Academy of Sciences of the United States of America, 115*(37), E8604-E8613. https://doi.org/10.1073/pnas.1800236115.

Huxman, T. E., Smith, M. D., Fay, P. A., Knapp, A. K., Shaw, M. R., Loik, M. E., et al. (2004) Convergence across biomes to a common rain-use efficiency. *Nature, 429*(6992), 651-654. https://doi.org/10.1038/nature02561.

Kirchner, J. W. and Allen, S. T. (2020) Seasonal partitioning of precipitation between streamflow and evapotranspiration, inferred from end-member splitting analysis. *Hydrology and Earth System Sciences, 24*(1), 17-39. https://doi.org/10.5194/hess-24-17-2020.

Liu, C., Sun, G., McNulty, S. G., Noormets, A., and Fang, Y. (2017) Environmental controls on seasonal ecosystem evapotranspiration/potential evapotranspiration ratio as determined by the global eddy flux measurements. *Hydrology and Earth System Sciences, 21*(1), 311-322. https://doi.org/10.5194/hess-21-311-2017.

Liu, Z., Yu, X., and Jia, G. (2019) Water uptake by coniferous and broad-leaved forest in a rocky mountainous area of northern China. *Agricultural and Forest Methodology, 265*, 381-389. https://doi.org/10.1016/j.agrformet.2018.11.036

Lyapustin, A., Wang, Y. (2018). MCD19A1 MODIS/Terra+Aqua Land Surface BRF Daily L2G Global 500m and 1km SIN Grid V006. NASA EOSDIS Land Processes DAAC. Accessed 2023-04-09 from https://doi.org/10.5067/MODIS/MCD19A1.006.

Martino, G., Fontana, N., Marini, G., and Singh, V. P. (2013) Variability and Trend in Seasonal Precipitation in the Continental United States. *Journal of Hydrologic Engineering 16*(6), 630-640. https://doi.org/10.1061/(asce)he.1943-5584.0000677.

The MathWorks Inc. (2022) MATLAB Version R2022a. Natick, Massachusetts.

McCormick, E.L., Dralle, D.N., Hahm, W.J. et al. (2021) Widespread woody plant use of water stored in bedrock. *Nature, 597*, 225–229. https://doi.org/10.1038/s41586-021-03761-3

NEON (National Ecological Observatory Network). (2022a) NEON Aquatic Watershed. Data accessed from https://hub.arcgis.com/datasets/neon::neon-aquatic-watershed-2 on September 16, 2022.

NEON (National Ecological Observatory Network). (2022b) Stable isotopes in surface water (DP1.20206.001), RELEASE-2022. https://doi.org/10.48443/yz7h-f560.

NEON (National Ecological Observatory Network). (2022c) Discharge field collection (DP1.20048.001), RELEASE-2022. https://doi.org/10.48443/tys0-ze83.

Patrick, L., Cable, J., Potts, D., Ignace, D. Barron-Gafford, G., Griffith, A., et al. (2007) Effects of an increase in summer precipitation on leaf, soil, and ecosystem fluxes of CO2 and H2O in a sotol grassland in Big Bend Park, Texas. *Oecologia, 151*, 704-718. https://doi.org/10.1007/s00442-006-0621-y.

Poage, M. A., & Chamberlain, C. P. (2001) Empirical relationships between elevation and the stable isotope composition of precipitation and surface waters: Considerations for studies of paleoelevation change. *American Journal of Science, 301*(1), 1-15. https://doi.org/10.2475/ajs.301.1.1.

Potapov, P., Li, X., Hernandez-Serna, A., Tyukavina, A., Hansen, M.C., Kommareddy, A., et al. (2020) Mapping and monitoring global forest canopy height through integration of GEDI and Landsat data. *Remote Sensing of Environment*, 112165. https://doi.org/10.1016/j.rse.2020.112165.

PRISM Climate Group (2014) Oregon State University, https://prism.oregonstate.edu, data created 4 Feb 2014, accessed 14 Feb 2023.

Reynolds, J. F., Kemp, P. R., Ogle, K., and Fernandez, R. J. (2004) Modifying the 'pulse-reserve' paradigm for deserts of North America: Precipitation pulses, soil water, and plant responses. *Oecologia, 141*(2), 194-210. https://doi.org/10.1007/s00442-004-1524-4.

Rhea, S. (2023) NEON Continuous Discharge Evaluation. *Hydroshare*. http://www.hydroshare.org/resource/1a388391632f4277992889e2de152163.

Sánchez-Murillo, R., Durán-Quesada, A. M., Esquivel-Hernández, G., Rojas-Cantillano, D., Birkel, C., Welsh, K., et al. (2019) Deciphering key processes controlling rainfall isotopic variability during extreme tropical cyclones. *Nature Communications, 10*, 4321. https://doi.org/10.1038/s41467-019-12062-3.

U.S. Geological Survey (2019) 3D Elevation Program 1 Arc Second Resolution Digital Elevation Model (published 20200406) accessed November 16, 2021, at URL https://apps.nationalmap.gov/downloader.

Van Rossum, G., & Drake Jr, F. L. (2009) Python 3 Reference Manual. Scotts Valley, CA: CreateSpace.

Vose, R. S., Applequist, S., Squires, M., Durre, I., Menne, M. J., Williams, C. N. Jr, et al. (2014) NOAA Monthly U.S. Climate Gridded Dataset (NClimGrid), Version 1. Average Summer and Winter Precipitation Trends. *NOAA National Centers for Environmental Information*. https://doi.org/10.7289/V5Sx6B56. 4/2/2023.

4. Thesis Conclusion

In chapter 2, we found that evapotranspiration (ET) was primarily composed of summer precipitation at the small, humid Rietholzbach watershed. We found that ET amount seems largely insensitive to variations in summer or winter precipitation. We surprisingly found that the sourcing of ET from summer versus winter precipitation was more evidently related to variations in winter precipitation amount, with winter precipitation seemingly contributing from zero up to ~50% of ET. Given that ET is relatively consistent, this implies that summer precipitation supplies the rest (50 to 100%). These variations in the partitioning of winter precipitation are likely driven by changes in transpiration rather than evaporation since most evaporation occurs in summer and is composed of recent precipitation.

In chapter 3, we found that climate and vegetation variables are related to partitioning fractions. A stepwise inverse-error regression modeling the fraction of summer precipitation to ET selected the following variables: coefficient of variation of chlorophyll carotenoid index, mean annual precipitation, minimum enhanced vegetation indices (EVI), and EVI area-under-the-curve. The model for the fraction of ET from summer precipitation selected the following variables: the ratio of summer precipitation to annual precipitation and minimum EVI. The selection of minimum EVI in both models supports our hypothesis that vegetation indices of health, density, and greenness are strong predictors of precipitation partitioning with negative effects on the relative flux of summer precipitation to ET. Our hypothesized mechanism was that ecosystems with less access to stored winter precipitation would experience drops in

vegetation health and greenness due to water stress as soil dries throughout the summer. However, the bimodal distribution of minimum EVI implies that these trends may be primarily driven by the categorical effect of evergreen versus deciduous vegetation which was not tested.

Overall, the findings produced in this thesis were exploration-motivated and they yielded new insights. However, it remains clear that uncertainty management is a challenge when using end-member splitting to compare hydrological behavior, and especially vegetation controls over hydrological behavior, across years and among sites.

Appendix 1: Supplemental Figures to Section 2. Research Chapter 1

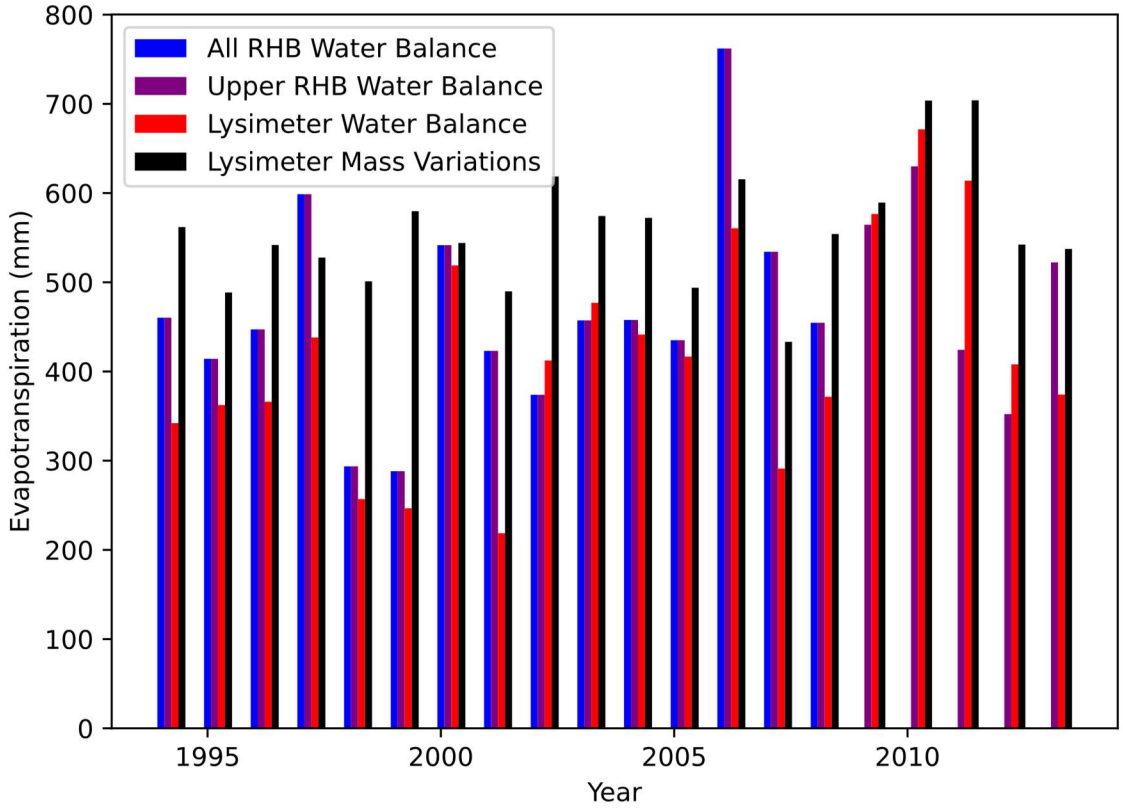

Figure S1 Bar plot showing annual evapotranspiration calculated by water-balance from All RHB in blue, Upper RHB in purple, and Lysimeter in red, and annual evapotranspiration calculated from lysimeter mass variations in black. Upper RHB is not included because the upper gauge was unreliable, so All RHB area-averaged runoff volumes were used instead. Each year represents a water year starting in October of the year on the x-axis and ending in September of the following year. Evapotranspiration from lysimeter mass variations shows the most consistency and is considered the most accurate. The standard error of the mean is 30.2 for All RHB Water Balance, 25.4 for Upper RHB Water Balance, 27.6 for Lysimeter Water Balance, and 15.0 for Lysimeter Mass Variations.

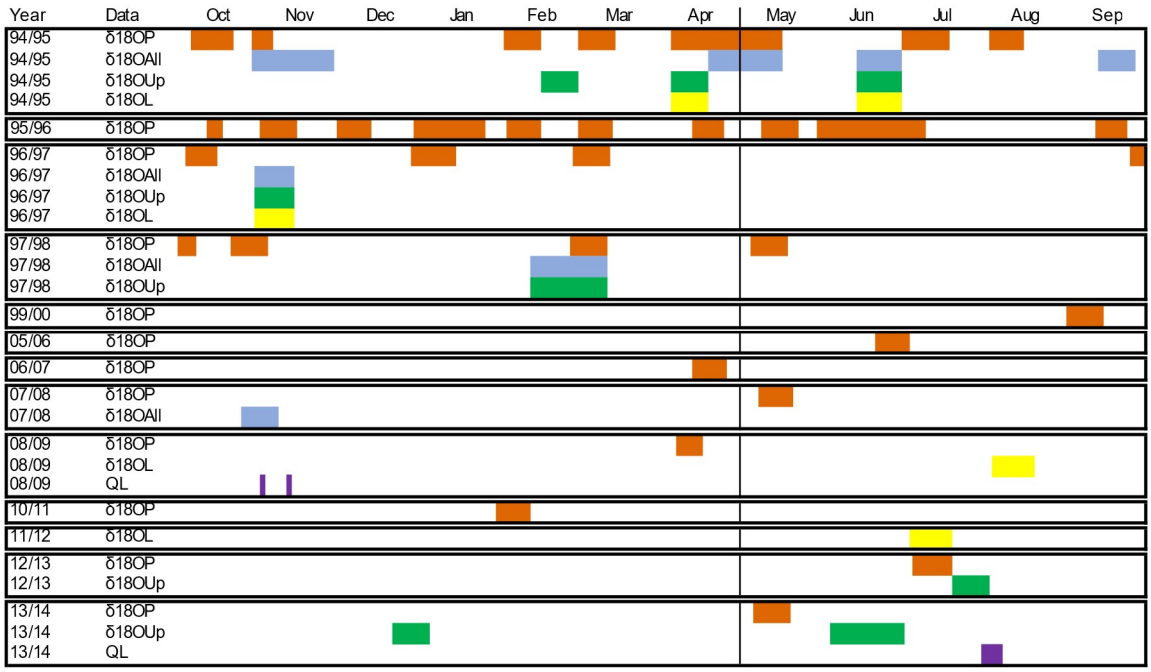

Figure S2 Colors show which days were missing isotope or flux data for each hydrologic year with orange representing precipitation isotope values (δ18OP), blue representing lower gauge isotope values (δ18OAll), green representing upper gauge isotope values (δ18OUp), yellow representing lysimeter isotope values (δ18OL), and purple representing lysimeter seepage amounts (QL). The vertical line represents the split between the winter and summer seasons.

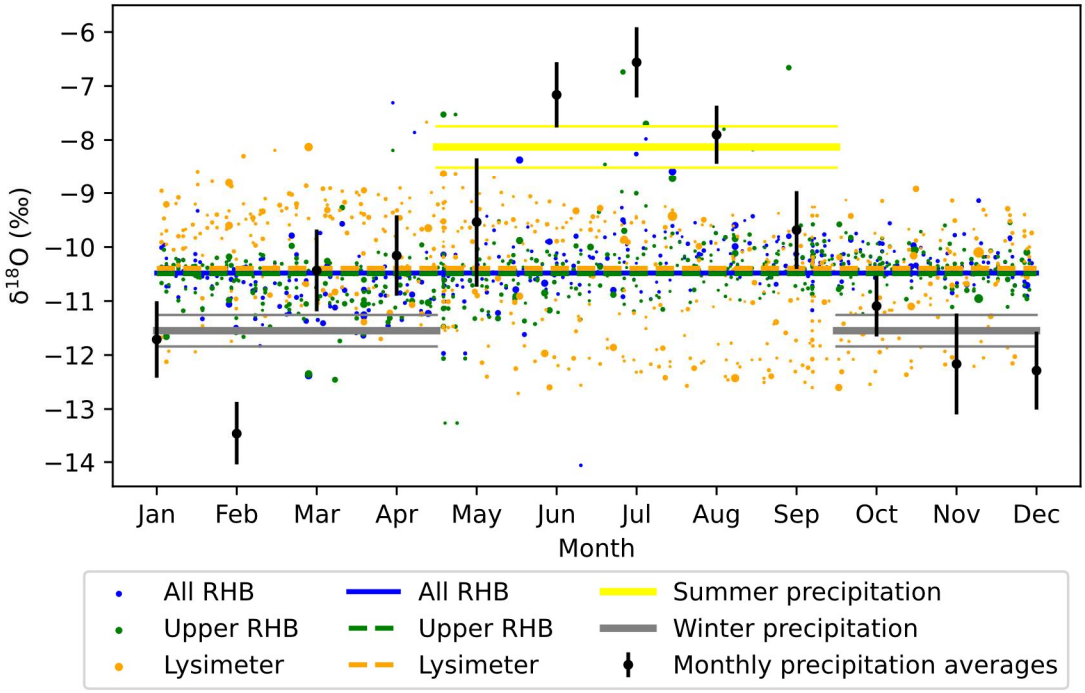

Figure S3 All $\delta^{18}O$ values of runoff and month- or season-averaged precipitation throughout the sampling period. Precipitation $\delta^{18}O$ (1994-2014) is shown as black dots with vertical lines representing monthly amount-weighted means and standard errors, and as horizonal yellow (summer) and grey (winter) lines representing seasonal weighted means and standard errors. Individual runoff measurements are shown in blue for the lower gauge (All RHB), orange for the upper gauge (Upper RHB), and green for the lysimeter, with marker sizes reflecting the runoff rate associated with each measurement. Runoff-weighted long-term mean $\delta^{18}O$ values are displayed as a blue line (All RHB) and a green line (Upper RHB and Lysimeter; Upper and Lysimeter values overlap such that they are indistinguishable at the resolution of this plot). Readers should note that runoff averages are nearer to the winter precipitation average than the summer precipitation average, which implies that streamflow is composed of more winter precipitation than summer precipitation. Readers should also note that the All RHB and Upper RHB runoff $\delta^{18}O$ values exhibit dampened and slightly lagged seasonal cycles relative to the monthly precipitation values, whereas the amplitude of the lysimeter values is more similar to that of precipitation but with an approximately 6-month phase lag, demonstrating contrasting transport and mixing behavior.

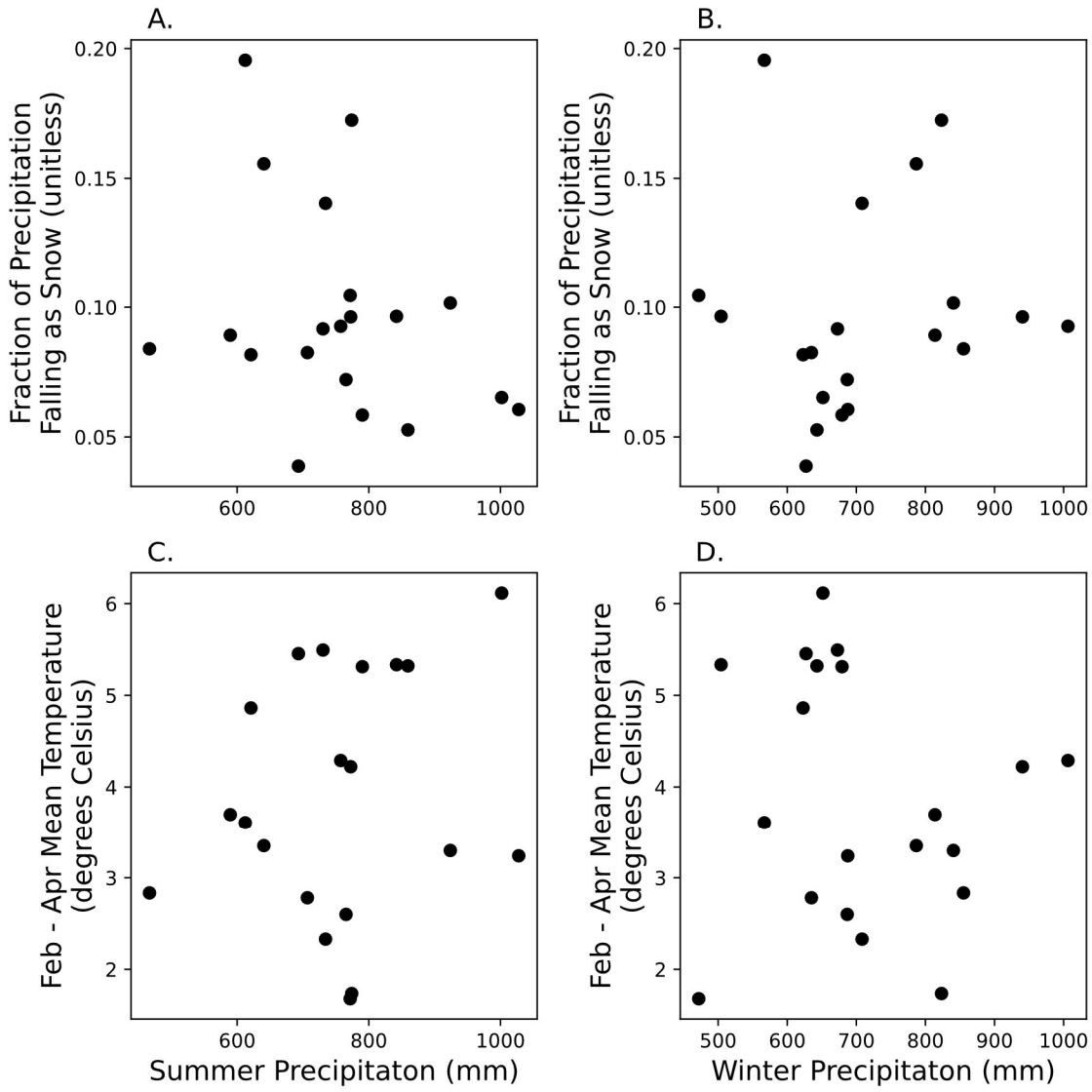

Figure S4 Plot of summer and winter precipitation amounts versus the fraction of precipitation falling as snow (when the daily average air temperature is at or below 2 degrees Celsius) and the February through April mean temperature in degrees Celsius. None of the plots show a significant trend ($p > 0.1$).

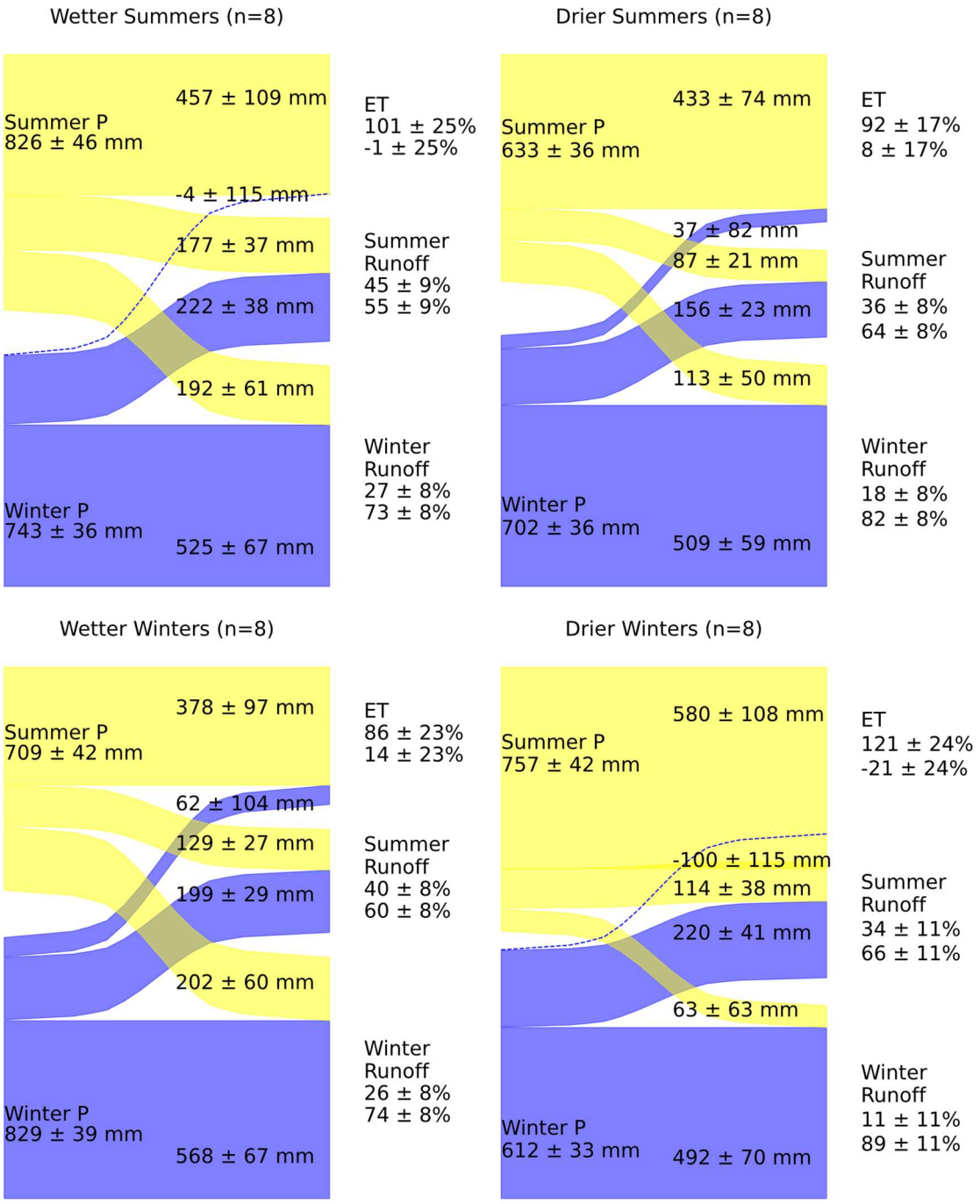

Figure S5 Summer and winter precipitation split into evapotranspiration, summer runoff, and winter runoff for the years in which summer precipitation was greater than versus less than the median summer precipitation compared to years in which winter precipitation was greater than versus less than the median winter precipitation amount using the entire watershed (All RHB) dataset. Values are shown as annual averages with standard error. The yellow represents fluxes from summer precipitation and the blue represents fluxes from winter precipitation. The thickness of each line corresponds with the flux amount. Dashed lines represent negative averages.

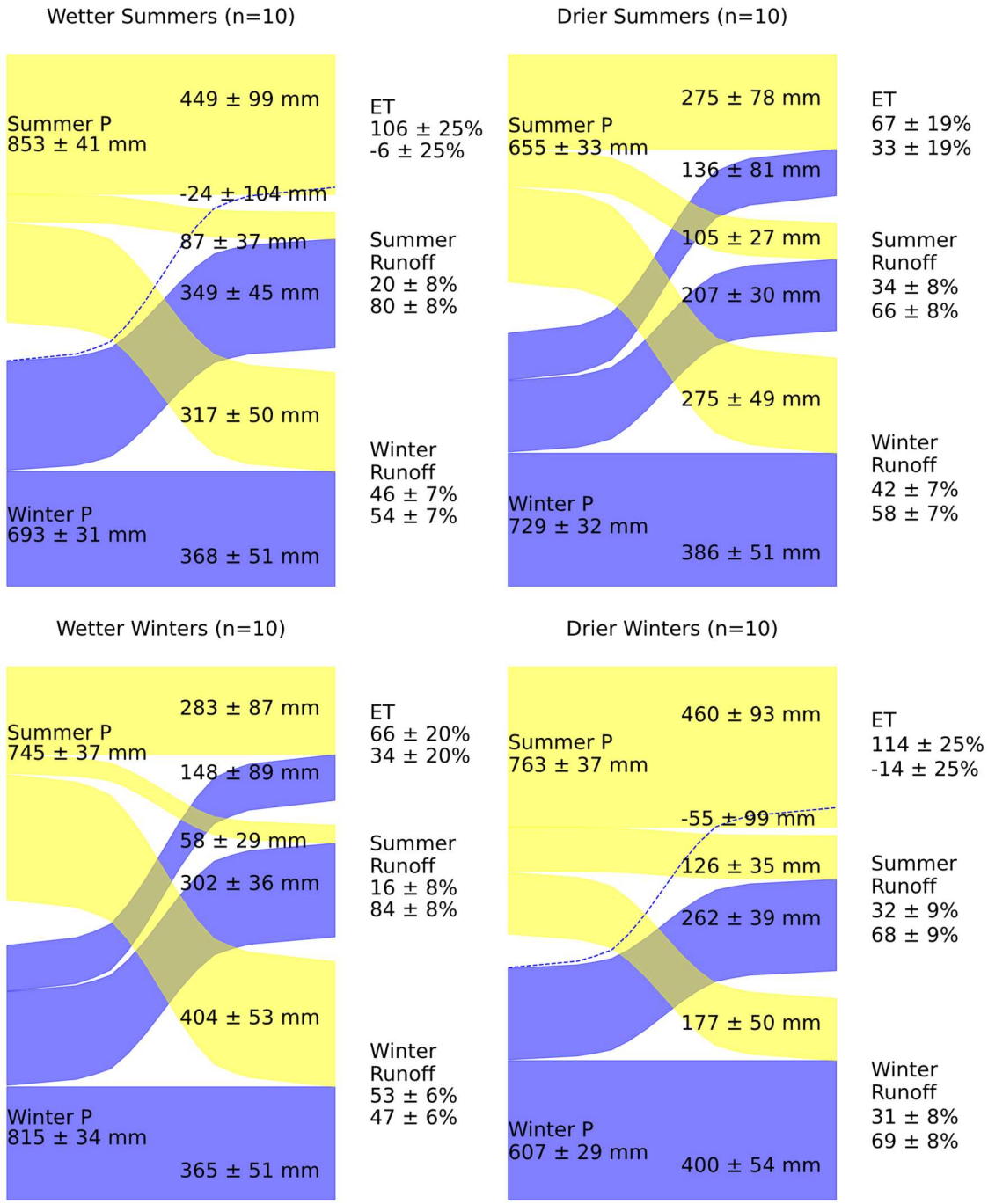

Figure S6 Summer and winter precipitation split into evapotranspiration, summer runoff, and winter runoff for the years in which summer precipitation was greater than versus less than the median summer precipitation compared to years in which winter precipitation was greater than versus less than the median winter precipitation amount using the lysimeter dataset. Values are shown as annual averages with standard error. The yellow represents fluxes from summer precipitation and the blue represents fluxes from winter precipitation. The thickness of each line corresponds with the flux amount. Dashed lines represent negative averages.

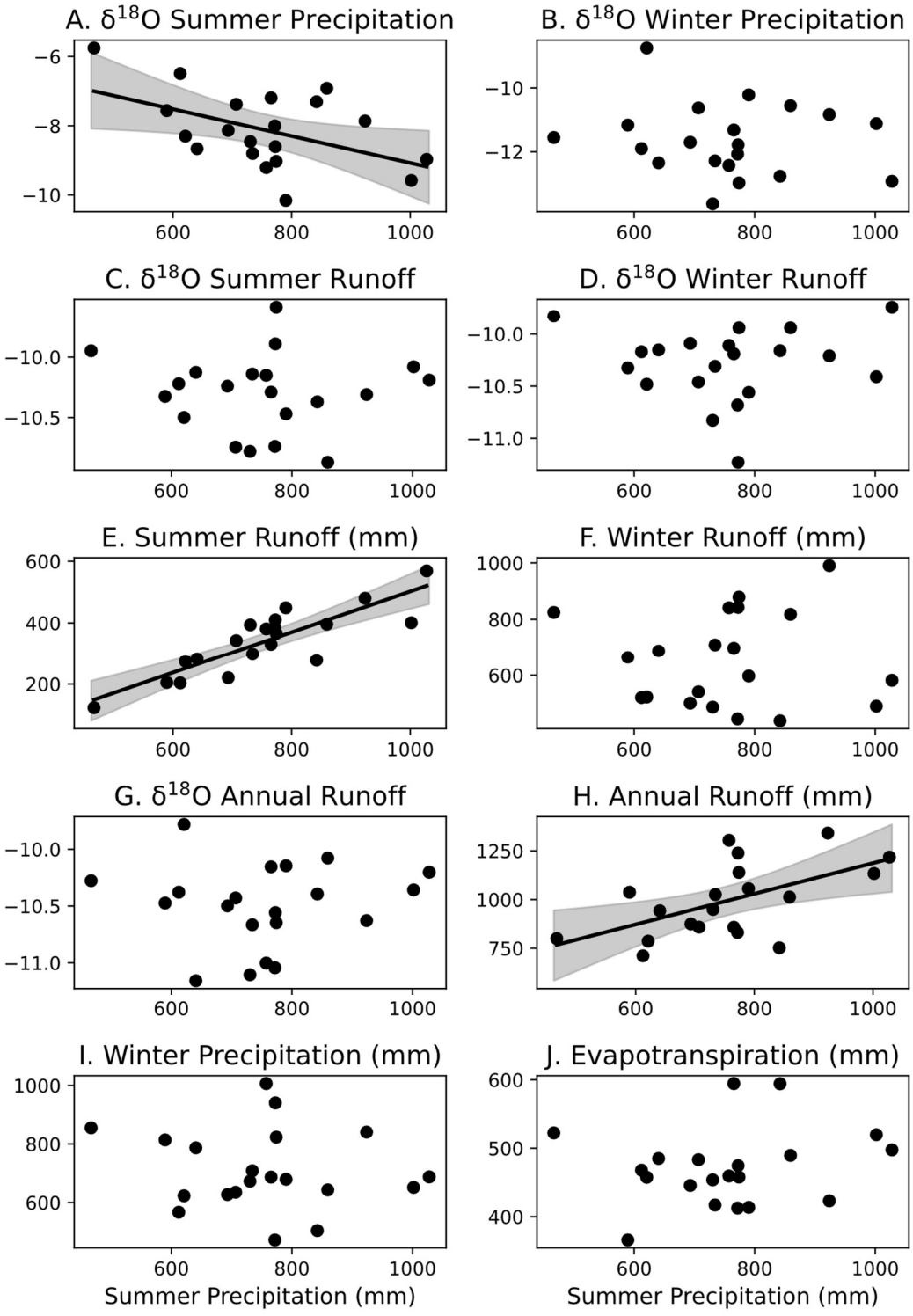

Figure S7 Correlations between summer precipitation amounts and Upper RHB annual values of variables in the end-member splitting and end-member mixing equations. Y-axis labels are shown as the title of each plot to improve readability. Trend lines and 95% confidence intervals are shown in the p-value is less than

0.1. Summer precipitation amount is negatively correlated with summer precipitation $\delta^{18}O$ (A), positively correlated with summer runoff amount (E), and positively correlated with annual runoff amount (H).

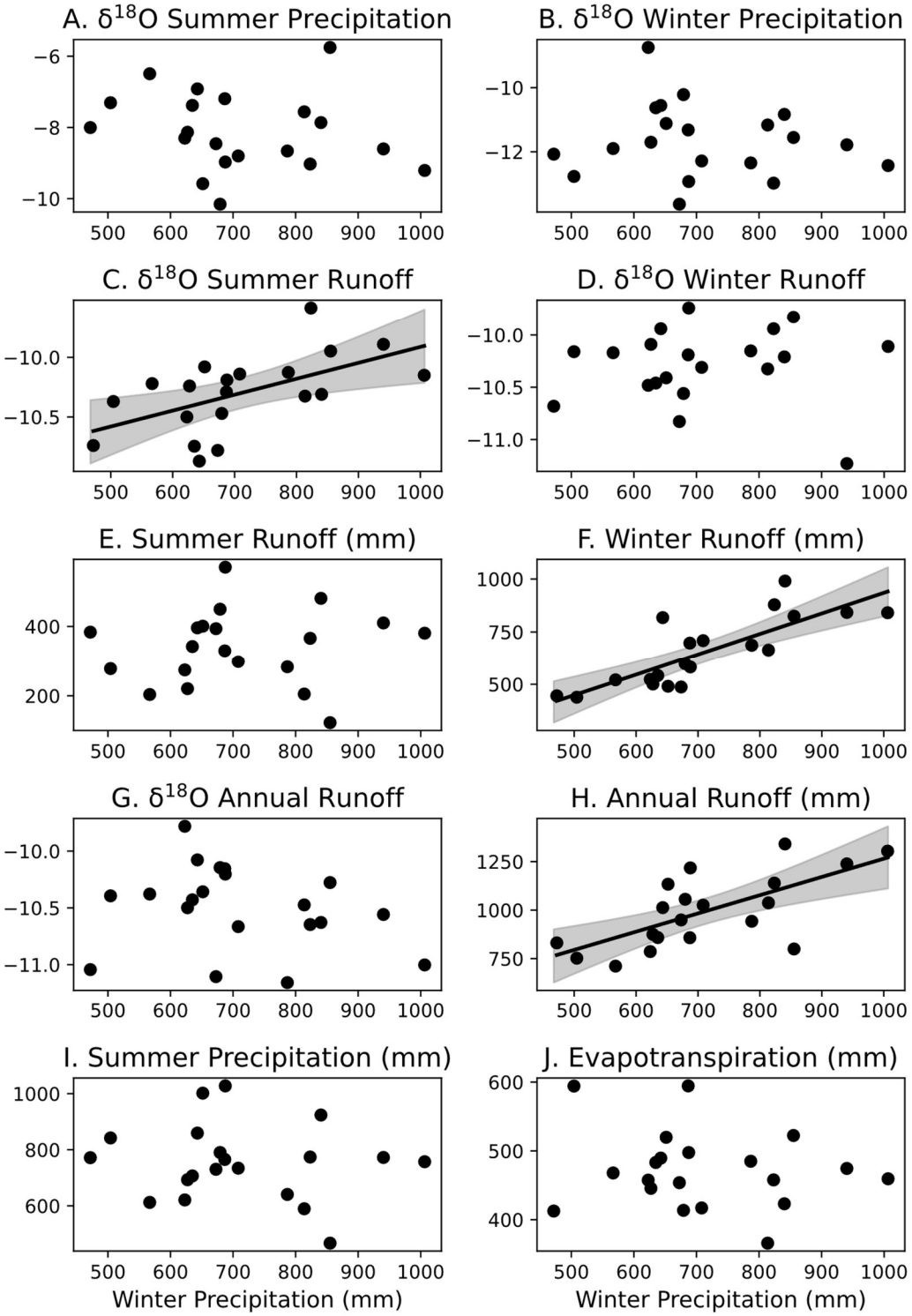

Figure S8 Correlations between winter precipitation amounts and Upper RHB annual values of variables in the end-member splitting and end-member mixing equations. Y-axis labels are shown as the title of each plot to improve readability. Trend lines and 95% confidence intervals are shown in the p-value is less than 0.1. Winter precipitation amount is positively correlated with summer runoff $\delta^{18}O$ (C), winter runoff amount (F), and annual runoff amount (H).

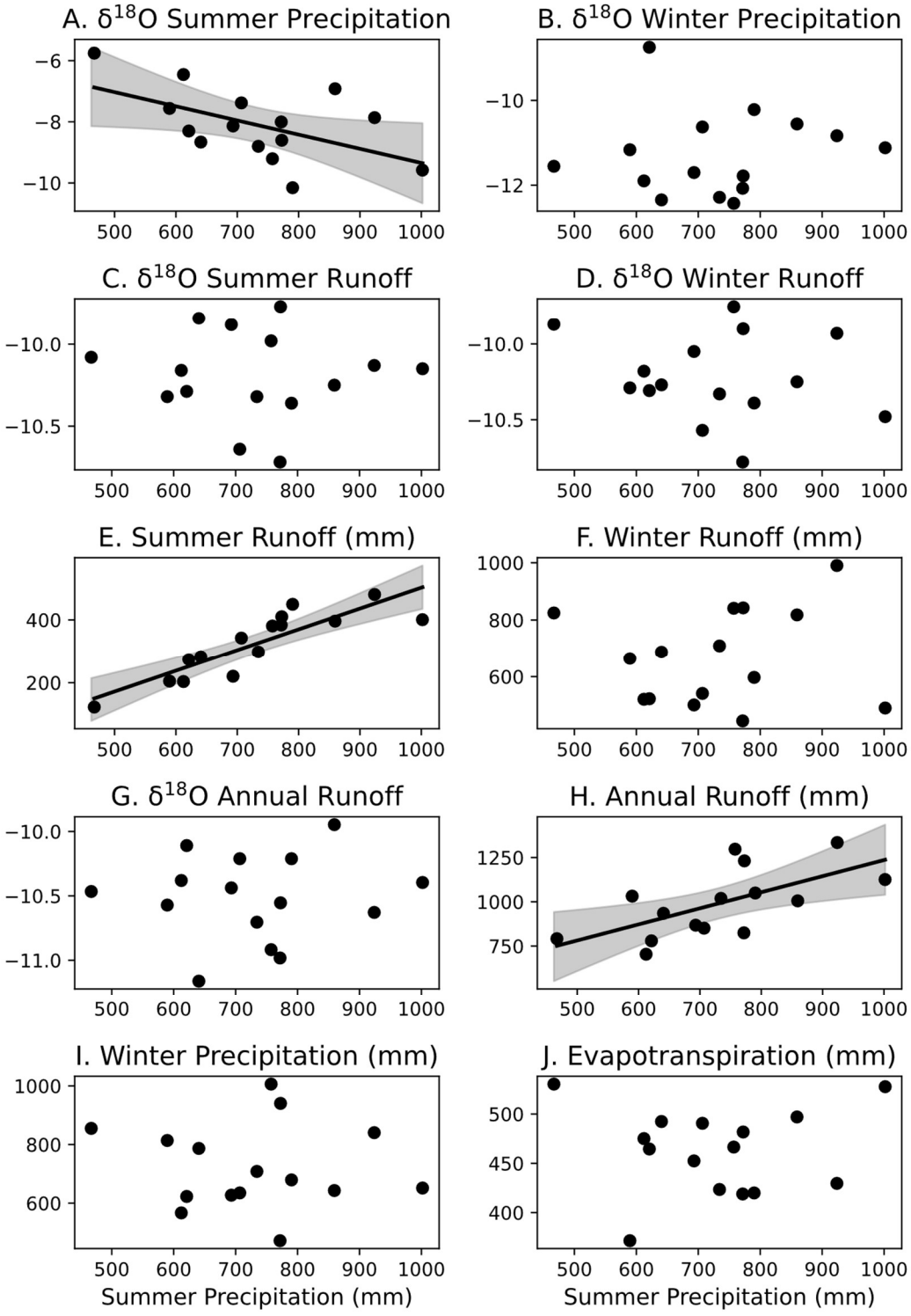

Figure S9 Correlations between summer precipitation amounts and All RHB annual values of variables in the end-member splitting and end-member mixing equations. Y-axis labels are shown as the title of each plot to improve readability. Trend lines and 95% confidence intervals are shown in the p-value is less than

0.1. Summer precipitation amount is negatively correlated with summer precipitation $\delta^{18}O$ (A), positively correlated with summer runoff amount (E), and positively correlated with annual runoff amount (H).

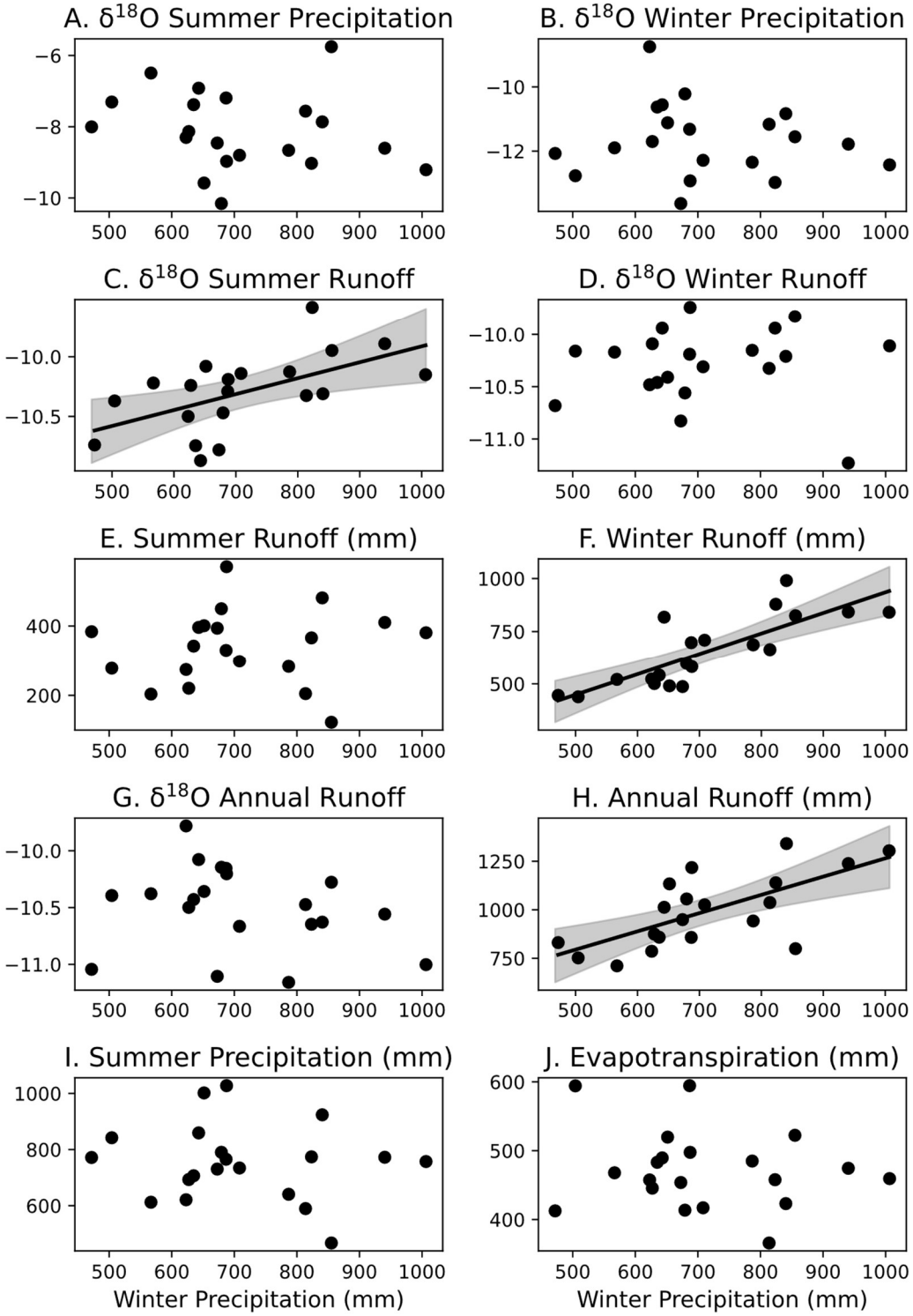

Figure S10 Correlations between winter precipitation amounts and All RHB annual values of variables in the end-member splitting and end-member mixing equations. Y-axis labels are shown as the title of each plot to improve readability. Trend lines and 95% confidence intervals are shown in the p-value is less than 0.1. Winter precipitation amount is positively correlated with summer runoff $\delta^{18}O$ (C), winter runoff $\delta^{18}O$ (D), winter runoff amount (F), and annual runoff amount (H).

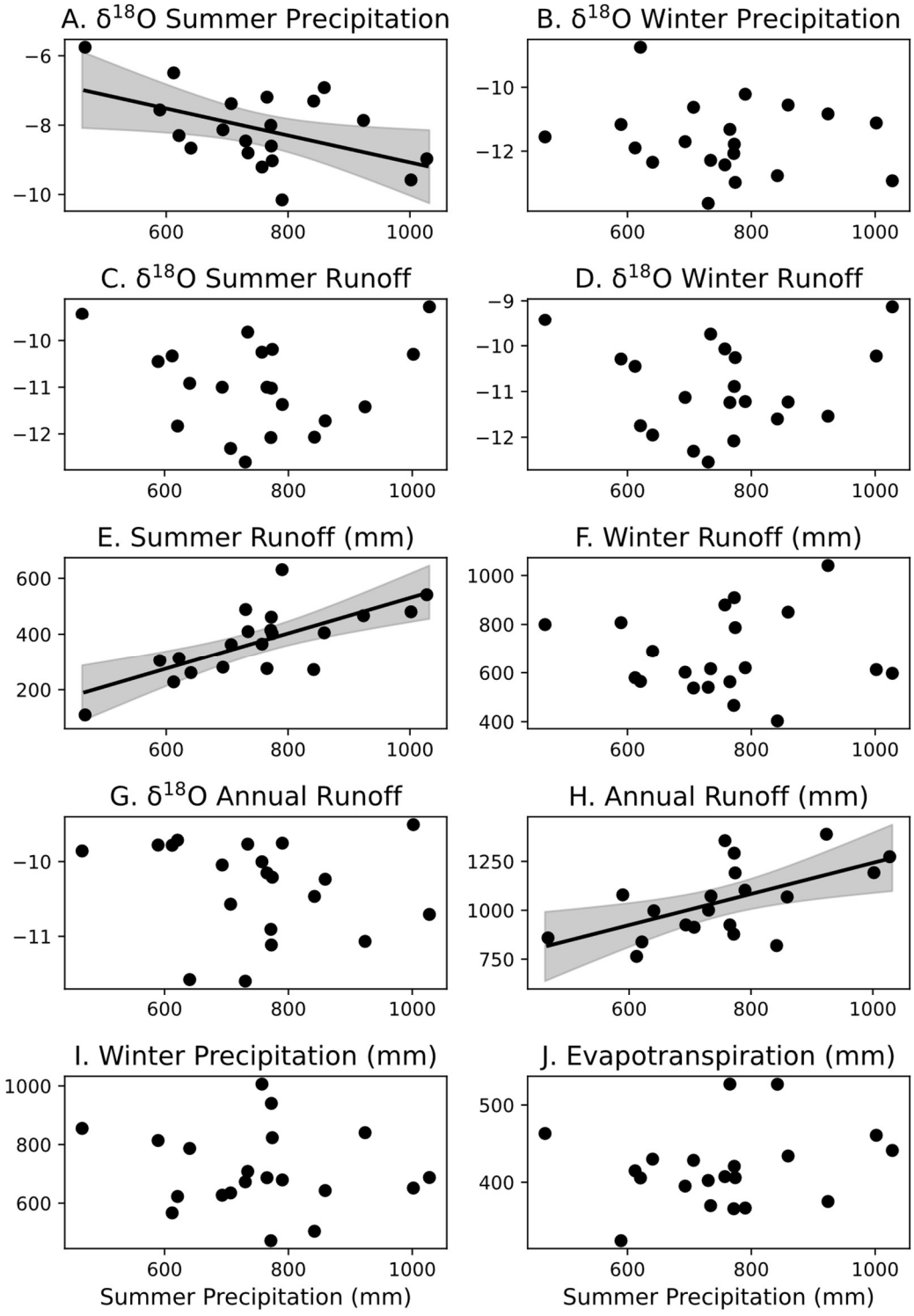

Figure S11 Correlations between summer precipitation amounts and Lysimeter annual values of variables in the end-member splitting and end-member mixing equations. Y-axis labels are shown as the title of each plot to improve readability. Trend lines and 95% confidence intervals are shown in the p-value is less than

0.1. Summer precipitation amount is negatively correlated with summer precipitation $\delta^{18}O$ (A), positively correlated with summer runoff amount (E), and positively correlated with annual runoff amount (H).

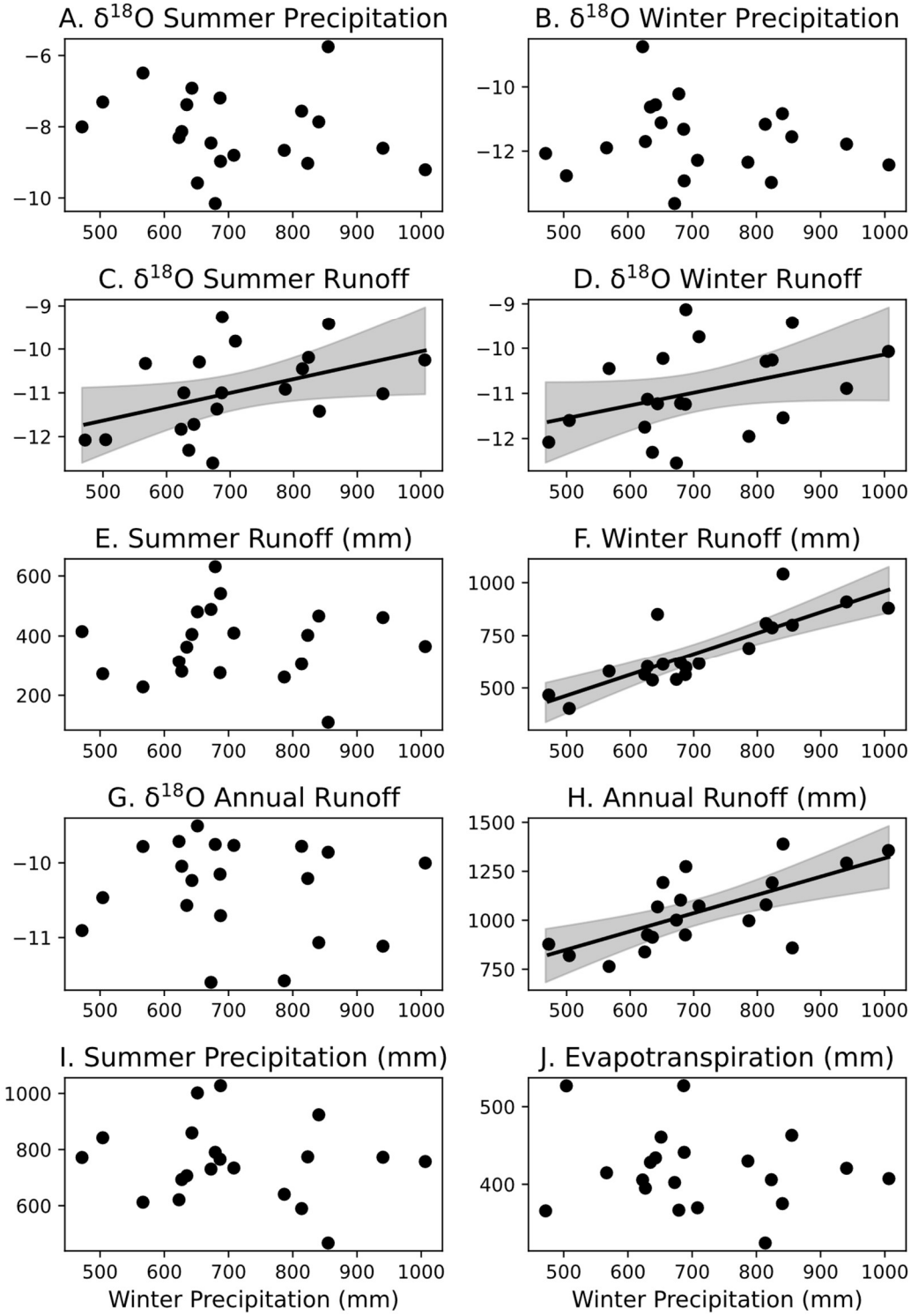

Figure S12 Correlations between winter precipitation amounts and Lysimeter annual values of variables in the end-member splitting and end-member mixing equations. Y-axis labels are shown as the title of each plot to improve readability. Trend lines and 95% confidence intervals are shown in the p-value is less than 0.1. Winter precipitation amount is positively correlated with summer runoff $\delta^{18}O$ (C), winter runoff $\delta^{18}O$ (D), winter runoff amount (F), and annual runoff amount (H).

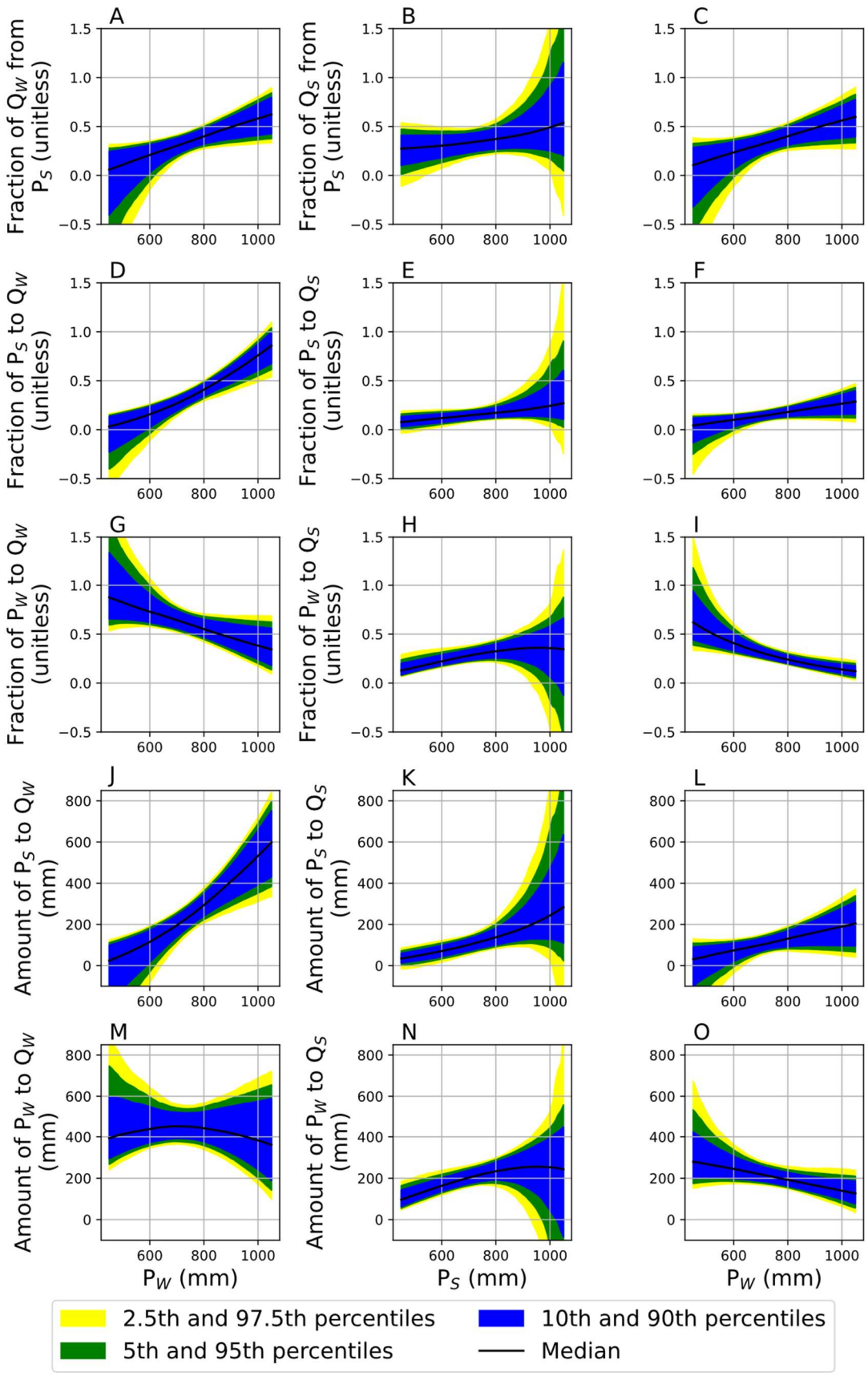
A
B
C
D
E
F
G
H
I
J
K
L
M
N
O
Fraction of Q_W from P_S (unitless)
Fraction of Q_S from P_S (unitless)
Fraction of P_S to Q_W (unitless)
Fraction of P_S to Q_S (unitless)
Fraction of P_W to Q_W (unitless)
Fraction of P_W to Q_S (unitless)
Amount of P_S to Q_W (mm)
Amount of P_S to Q_S (mm)
Amount of P_W to Q_W (mm)
Amount of P_W to Q_S (mm)
P_W (mm)
P_S (mm)
P_W (mm)
2.5th and 97.5th percentiles
10th and 90th percentiles
5th and 95th percentiles
Median

Figure S13 Fractions and amounts of precipitation partitioning into summer and winter runoff with summer precipitation (mm) and winter precipitation (mm) on the x-axis. These plots only show data from All RHB. The blue area covers the 10^{th} to the 90^{th} percentiles of the 3000 bootstrapping iterations. The green area extends to the 5^{th} and 95^{th} percentiles while the yellow area extends to the 2.5^{th} and 97.5^{th} percentiles.

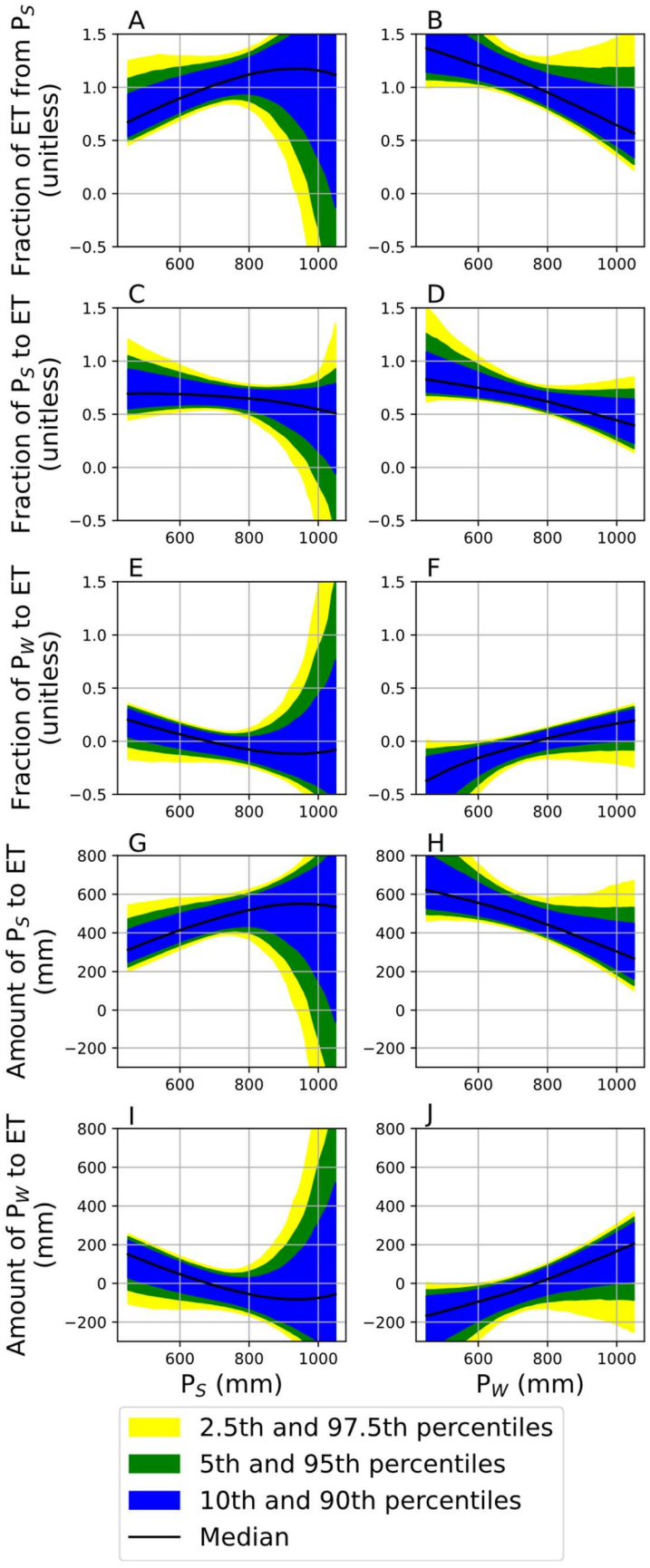
A
B
C
D
E
F
G
H
I
J
Fraction of ET from P_S (unitless)
Fraction of P_S to ET (unitless)
Fraction of P_W to ET (unitless)
Amount of P_S to ET (mm)
Amount of P_W to ET (mm)
P_S (mm)
P_W (mm)
2.5th and 97.5th percentiles
5th and 95th percentiles
10th and 90th percentiles
Median

Figure S14 Fractions and amounts of precipitation partitioning into evapotranspiration with summer precipitation (mm) and winter precipitation (mm) on the x-axis. These plots only show data from All RHB. The blue area covers the 10^{th} to the 90^{th} percentiles of the 3000 bootstrapping iterations. The green area extends to the 5^{th} and 95^{th} percentiles while the yellow area extends to the 2.5^{th} and 97.5^{th} percentiles.

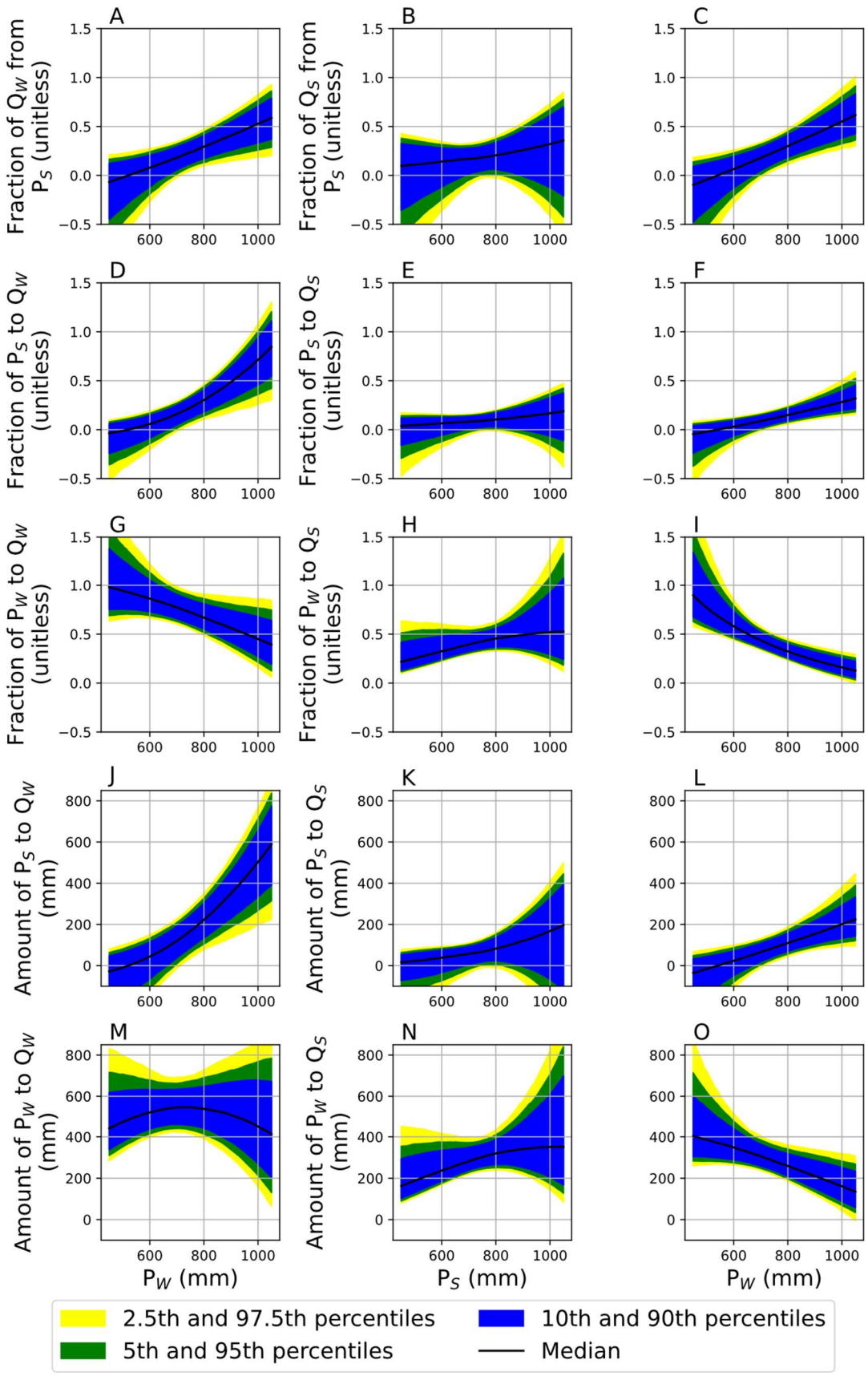
A
B
C
D
E
F
G
H
I
J
K
L
M
N
O
Fraction of Q_W from P_S (unitless)
Fraction of Q_S from P_S (unitless)
Fraction of P_S to Q_W (unitless)
Fraction of P_S to Q_S (unitless)
Fraction of P_W to Q_W (unitless)
Fraction of P_W to Q_S (unitless)
Amount of P_S to Q_W (mm)
Amount of P_S to Q_S (mm)
Amount of P_W to Q_W (mm)
Amount of P_W to Q_S (mm)
P_W (mm)
P_S (mm)
P_W (mm)
2.5th and 97.5th percentiles
10th and 90th percentiles
5th and 95th percentiles
Median

Figure S15 Fractions and amounts of precipitation partitioning into summer and winter runoff with summer precipitation (mm) and winter precipitation (mm) on the x-axis. These plots only show data from the lysimeter. The blue area covers the 10^{th} to the 90^{th} percentiles of the 3000 bootstrapping iterations. The green area extends to the 5^{th} and 95^{th} percentiles while the yellow area extends to the 2.5^{th} and 97.5^{th} percentiles.

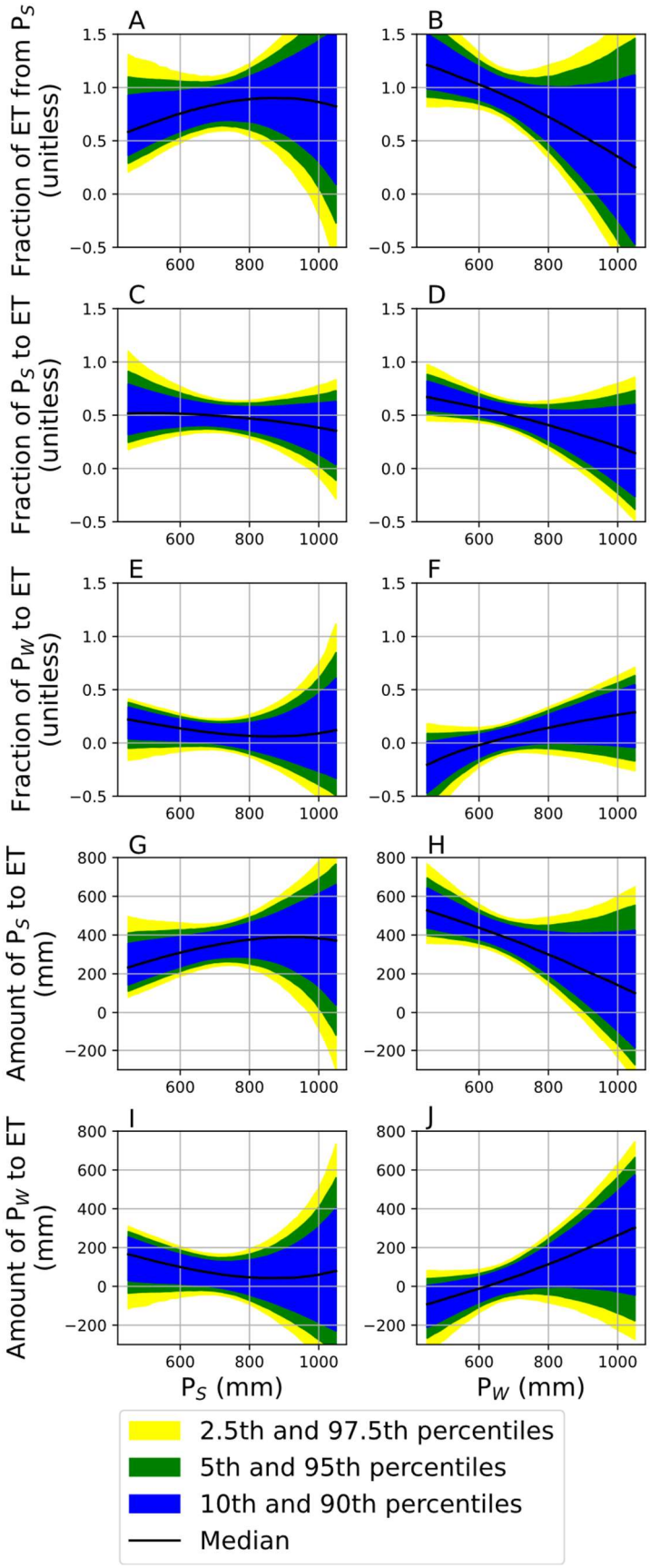
A
B
C
D
E
F
G
H
I
J
Fraction of ET from P_S (unitless)
Fraction of P_S to ET (unitless)
Fraction of P_W to ET (unitless)
Amount of P_S to ET (mm)
Amount of P_W to ET (mm)
P_S (mm)
P_W (mm)
2.5th and 97.5th percentiles
5th and 95th percentiles
10th and 90th percentiles
Median

Figure S16 Fractions and amounts of precipitation partitioning into evapotranspiration with summer precipitation (mm) and winter precipitation (mm) on the x-axis. These plots only show data from the lysimeter. The blue area covers the 10^{th} to the 90^{th} percentiles of the 3000 bootstrapping iterations. The green area extends to the 5^{th} and 95^{th} percentiles while the yellow area extends to the 2.5^{th} and 97.5^{th} percentiles.